THE UNIVERSITY OF MICHIGAN
COLLEGE OF LITERATURE, SCIENCE, AND THE ARTS
Department of Physics

Technical Report No. 1

HIGH RESOLUTION ELECTRIC FIELD INDUCED INFRARED ABSORPTION SPECTRA OF H_2 AND D_2

C. H. Church

UMRI Project 2609

under contract with:

DEPARTMENT OF THE AIR FORCE
AIR RESEARCH AND DEVELOPMENT COMMAND
AIR FORCE CAMBRIDGE RESEARCH CENTER
GEOPHYSICS RESEARCH DIRECTORATE

CONTRACT NO AF 19(604)-2071
BEDFORD, MASSACHUSETTS

administered by:

THE UNIVERSITY OF MICHIGAN RESEARCH INSTITUTE
ANN ARBOR

January 1959

TABLE OF CONTENTS

LIST OF TABLES

LIST OF FIGURES

Figure

Page

ABSTRACT

A high-resolution study has been made of the electric field-induced vibration-rotation absorption spectra of H_2 and D_2. The induced absorption was modulated at 90 cps by square wave fields of 100,000 volts/cm maximum value applied to a one meter long Stark cell of the light guide type operated at pressures up to thirty atmospheres. The spectrum was analyzed by a F/15 vacuum grating spectrograph of the Ebert design using a 200 mm wide grating with 300 lines per mm double passed. The radiation was detected by lead sulfide photoconductive cells cooled by liquid nitrogen. The small modulated component of the output of the detector was isolated and amplified electronically. White light fringes produced in a Fabry-Perot etalon were used for the determination of the line positions. The absolute intensities of the lines were measured for specific polarization directions in order to calculate the polarizability components of the molecules. The spectral resolution varied between 0.1 and 0.2 cm^{-1}. The probable error in the determination of the transition frequencies was 0.02 cm^{-1}, and that for the values of the polarizability components was 3 percent.

The ν_{0-1} transitions observed for H_2 included 6 Q branch lines, 4 S lines, and 1 O line that was largely obscured; and the ν_{0-2} transitions, 3 Q lines. For D_2, 5 Q and 5 S lines were detected in the fundamental, and 3 Q lines in the overtone. The spectral resolution used (0.1 to 0.2 cm^{-1}) was comparable to the line widths. A new set of molecular constants was calculated for both H_2 and D_2 to best fit the data, generally within 0.01 cm^{-1}. They differed only slightly from those given by Stoicheff. The ratio of the equilibrium vibrational frequencies of H_2 and D_2 could not be compared closely with the ratio determined by the reduced masses of the molecules because of the lack of a reliable value of ν_{0-3} for D_2. The values obtained for the polarizability matrix elements α_{01} and γ_{01} for both molecules are in excellent agreement with the most recent experimental determinations from static electric field-induced absorption and photoelectric Raman and Rayleigh scattering data.

It is concluded that the modulated electric field absorption technique offers the highest sensitivity in the detection of weak vibration-rotation transitions in H_2 and D_2, and yields values of line positions and intensities of comparable or greater accuracy than other available methods. Several changes are suggested that should further improve the technique.

I. INTRODUCTION

Although Condon (1) had predicted that absorption by a normally inactive molecular vibration could be induced by the application of a strong electric field, the phenomenon was not observed until 1953 by Crawford and Dagg (2) for H_2, using a static electric field. Terhune (3) in the past year studied the vibration-rotation absorption bands of H_2 and D_2 with a spectral resolution of 1 to 2 cm^{-1} using a low-frequency alternating electric field to modulate the absorption and then selectively amplifying only the small A.C. modulated portion of the output signal from the detector. His results showed the feasibility of the quantitative investigation of such normally inactive molecular vibrations through their electric field-induced spectra. The same technique had been suggested earlier by Woodward (4).

The electric field-induced spectrum is analogous to the Raman spectrum in that a D.C. or low-frequency electric field induces a dipole moment in the molecule in the same fashion that the very-high-frequency electric field of a photon induces a dipole moment in the case of the Raman spectrum (1). (See also the theory of the

Raman spectrum by Plazcek [5].) The selection rules and intensity calculations are very similar in the two cases, differing only in the effects due to the directions of polarization and observation relative to that of the incident radiation, and to the frequency dependence of an absorption versus an emission process.

The present work is an attempt to extent Terhune's work so as to exploit this method. H_2 and D_2 were again used as test cases, although the same apparatus could be used with few changes for the measurement of similar inactive vibrations in a large number of molecules. The major factors involved in this effort to enhance the performance were: (a) the use of the vacuum Ebert multipass grating spectrometer for high spectral resolution as well as the elimination of the interference of atmospheric water-vapor absorption bands; (b) a high-pressure Stark cell of one meter length of the light guide type having a uniform spacing of the electrodes and a high efficiency with respect to transmission; (c) a square-wave high-voltage power supply to maintain a constant electric field between the electrodes so that accurate values of the intensities of the absorption lines and hence the polarizability components could be measured; (d) the use of lead sulfide photoconductive detectors that were cooled to dry ice and liquid air temperatures to enhance their response; and (e) the use of a Fabry-Perot etalon that generated

equally spaced white-light fringes to calibrate the spectra to a higher accuracy than is possible using the grating drive alone.

By virtue of these instrumental features, it was hoped that information on the vibrational-rotational energy levels and the polarizability of molecular hydrogen and deuterium would be obtained in greater detail and accuracy than by other methods; namely, electronic-emission spectra, Raman spectra, and vibrational quadrupole spectra.

These other methods possess certain advantages and disadvantages when they are compared with electric field-induced spectra. The electronic-emission spectra of both H_2 and D_2 lie in the vacuum ultraviolet. Transitions from quite high vibrational states are observed, although only low rotational states ($J = 4$ or 5), characteristic of a room-temperature distribution, are found (the small number of rotational levels with an appreciable population being due to the small moment of inertia involved). Absolute wave-length measurements in the vacuum in ultraviolet are difficult, and extraordinary precision is necessary in order to determine accurately the vibrational and rotational constants since the electronic contribution to the energy is so much larger relatively. Jeppesen (6, 7) gave data for the first five vibrational states of H_2 and for nine vibrational states of D_2, with an accuracy of the order of 1 cm^{-1}. A considerable improvement could be realized at the present time; for example,

in Herzberg's (8) measurements on atomic hydrogen in the same spectral region a probable error of 0.02 cm^{-1} is reported. The intensity of the electronic-emission spectrum is overwhelmingly greater (by a factor of 10^6 or more) than that of the Raman, quadrupole, or field-induced spectra.

The recent Raman work by Stoicheff (9) has given the most accurate values of the molecular constants of H_2 and D_2 for the $v = 0$ and $v = 1$ states. He observed four pure rotation lines and four lines in the Q branch of the fundamental vibration for H_2 with a probable error of 0.02 cm^{-1}; and for D_2, five pure rotation lines and five Q branch lines, good to 0.05 cm^{-1}. The exciting radiation was either the 4358 Å or 4046 A mercury line. Photographic recording permitted the use of long integration times (up to 36 hours), and the wave-length standards available in the visible gave a straight forward calibration technique. Gas pressures of one to two atmospheres were used in a multipassed high-efficiency Raman cell of 80 cm illuminated length.

Information on several components of the polarizability tensor of the molecule can be obtained from its scattering. A measurement of the absolute intensity of Raman scattering does not appear possible. However, the ratios of the anisotropic polarizability to the isotropic polarizabilities, $\left|\frac{\gamma_{00}}{\alpha_{00}}\right|$ and $\left|\frac{\gamma_{01}}{\alpha_{01}}\right|$, can be calculated from

the depolarization of the Rayleigh and Raman scattering, respectively. In addition, the ratio of the intensity of Raman to Rayleigh scattering coupled with the value of α_{00} from refractive index data enables one to calculate α_{01}. These equations are discussed in detail in Chapter II. In this manner, Stansbury, Crawford, and Welsh (10) have obtained data for both H_2 and D_2. Problems in photographic intensity measurements along with the small value of the ratio of Raman to Rayleigh scattering limit the accuracy of their work, however. Yoshino and Bernstein (11) have recently published work on the photoelectric measurement of Raman intensities of a number of gases, including H_2 and D_2. Although done at low resolution, the probable error in the polarizability values is reduced to several percent.

Although molecular quadrupole absorption is extremely feeble, Herzberg (12) has observed photographically several lines in the first and second overtones of H_2 with the aid of extremely long path lengths, 1.2 kilometers and 4.5 kilometers, respectively, both at ten atmospheres pressure. He detected four lines in each band, one in each Q branch, and three in each S branch, with an accuracy of about 0.02 cm^{-1}. Conceivably, the fundamental could be sought out, yet it is of only approximately the same strength as the overtones because of the large mechanical and electrical anharmonicity of H_2, and also because the quadrupole absorption intensity varies as ν^3.

The latter effect would make it even more difficult to observe the quadrupole transitions of D_2 or other molecules.

The observations made by Crawford and Dagg (2) of the field-induced absorption of H_2 were complicated by the presence of a large background absorption arising in a similar manner from molecular fields during collisions between molecules. The brief time interval of the collision process leads to an extremely wide half-width for these pressure-induced lines. However, this background may shift the apparent position of the maxima of the static field-induced absorption lines. In addition, only the stronger lines can be distinguished from this background. Since the absorption must be appreciable to be distinguishable from the background, only the more intense lines are observable, and the absorption is in the nonlinear range so that absolute absorption strengths and hence polarizability values are difficult to determine. Crawford and MacDonald (13) published further results for static electric fields after measurements in the present work were completed. Their work was done at a resolution of 0.5 to 1 cm^{-1}, and frequency shifts from Stoicheff's Raman data of 0.1 to 0.2 cm^{-1} were reported for several lines ($Q_1[0]$, $Q_1[1]$, $Q_1[2]$, $Q_1[3]$, and $S_1[1]$ were observed). After extrapolation to zero absorption, values of the absorption coefficients were obtained and values were calculated to an estimated accuracy of

1 or 2 percent. A slight increase in absorption strength was noted for $Q_1(1)$ at higher pressures.

The hydrogen molecule has been the subject of extensive theoretical work due to its unique position as the simplest stable molecule. Although calculations of the energy levels have been made, they in no way rival the accuracy to the experimental values. On the other hand, theoretical and experimental values of the polarizability matrix elements are of comparable accuracy. The most complete theoretical treatment of these quantities has been given by Ishiguro, Arai, Mizushima, and Kotani (14). Their values of the average polarizability and the anisotropic component for the ground vibrational state (α_{00} and γ_{00}) agree closely with the experimentally determined values. However, for the polarizability elements involved in a transition between the ground and first excited vibrational state (α_{01} and γ_{01}), the various experimental values range between 10 and 40 percent below the calculated values. Considering that these quantities furnish a fairly sensitive test of the accuracy of the wave function selected, a reliable experimental determination was thought to be of value. The results by Yoshino and Bernstein and by Crawford and MacDonald have largely settled this question, however, by showing the calculated values to be in error.

For the present investigation, it was estimated from the available performance information on the spectrometer that at 0.1 cm^{-1} spectral resolution absorptions of one part in one thousand could be readily detected at a one-second response time. Using this value and Terhune's (3) data, it was predicted that with a one-meter absorption cell at thirty atmospheres pressure it would be possible to observe transitions an order of magnitude weaker than had been observed in the Raman effect of H_2 and D_2; for example, the lower lines of the S branch and several lines in the O branch of the fundamental, and possibly several lines in the Q branch of the first overtone. Further, it appeared that the frequencies could be measured to approximately 0.01 cm^{-1}.

Additionally, the absolute intensities of the lines could be determined with a reasonable accuracy so that α_{01} and γ_{01} could be evaluated within an error of several percent, both for H_2 and D_2.

II. THEORY OF ELECTRIC FIELD-INDUCED ABSORPTION SPECTRA

2.1 Line intensities and polarizabilities

The intensity I of light passing through an absorbing medium such as in the region of an absorption line may be expressed as

$$I(\nu) = I_0 e^{-\rho(\nu) L} \tag{1}$$

in which $\rho(\nu)$ is the absorption coefficient which is a function of the frequency of the light ν in wave numbers (cm^{-1}), L is the path length, and I_0 is the initial intensity of the light. When the product $\rho(\nu)L$ is small compared to one (which avoids any effects due to strong absorptions), the exponential may be approximated so that

$$\frac{I_0 - I(\nu)}{I_0} = \rho(\nu) L \tag{2}$$

In this experiment only low-level absorptions satisfying this were considered. Since an absorption line has a finite width, we must integrate equation 2 over the frequency range of the absorption line, the integral being denoted by the symbol A, which will be called the absorption strength:

$$A = \int_{\Delta\nu} \frac{I_o - I(\nu)}{I_o} d\nu = L \int_{\Delta\nu} \rho(\nu) d\nu \qquad (3)$$

The quantity on the left is experimentally measured as the area under the absorption line expressed in terms of the relative intensity and the wave-number interval. The integral $\int \rho(\nu)\, d\nu$ is known as the integrated absorption coefficient, symbolized by K, and can be expressed in terms of the dipole moment of the molecule and consequently the polarizability.

The integrated absorption coefficient K for any molecule with degenerate M levels, in plane polarized light, neglecting quadrupole and higher terms, is given by the expression:

$$K_{n\,v\,J}^{n'v'J'} = \frac{8\pi^3 N_{nvJ}}{hc(2J+1)} \nu_{n\,v\,J}^{n'v'J'} \sum_{M'} \sum_{M=-J}^{J} |\langle nvJM|\mu_w|n'v'J'M'\rangle|^2 \qquad (4)$$

where h is Planck's constant; c, the velocity of light; n, v, J, the electronic, vitrational, and rotation quantum numbers of the initial state; n', v', J', those of the final state, respectively; N_{nvJ}, the number of molecules in the initial state; $\nu_{nvJ}^{n'v'J'}$, the frequency difference between the initial and final states in wave numbers; M, the projection of J on the preferred axis; and μ_w, the component of the dipole moment in the direction of the electric field of the light vector (15). In the case of the field-induced spectra, the static electric field introduces a preferred axis in space, and the absorption

coefficient depends upon whether the electric field of the light is perpendicular or parallel to the static electric field.

In this investigation, no electronic transitions occurred, so that the electronic quantum number, n, remained constant; hence it will be dropped from the equations that follow.

In the case of degenerate M levels, the quantity N_{vJ}, the number of molecules in the initial state, is given by (16):

$$N_{vJ} = \frac{N\, g(J)\ (2J+1)\, e^{-W_{vJ}/kT}}{\sum g(J)\ (2J+1)\, e^{-W_{vJ}/kT}} = N\ f_{vJ} \qquad (5)$$

where N is the number of molecules per cm^3 under the experimental conditions and g(J) is the statistical weight or degeneracy of the levels due to nuclear spin. In H_2, g(J) is one for even J and three for odd J; in D_2, it is two for even J and one for odd J. W_{vJ} is the energy difference between the state vJ and the ground state. As the transitions considered here are all from the ground vibrational state, W_{vJ} is expressed in terms of the rotational constants B_o and D_o, and the zero point energy $G_{(1/2)}$:

$$W_{vJ} = [B_o J(J+1) - D_o J^2(J+1)^2]hc + G(\tfrac{1}{2}) \qquad (6)$$

The zero point energy cancels out when this is used in equation 5.

The theory of the induced dipole moment absorption will be specialized to the case of homonuclear diatomic molecules, which do not possess a permanent dipole moment because of their symmetry. The dipole moment μ_w is that induced by the static electric field, E, which will be considered to be in the z direction:

$$\mu_w = \alpha'_{wz} E_z \tag{7}$$

where w is the space-fixed direction of the incident light and α'_{wz} are the space-fixed components of the polarizability tensor. The polarizability of a molecule is usually expressed with respect to molecule-fixed axes, and the space-fixed components are related to the molecule-fixed components, α_{ij}, through the transformation:

$$\alpha'_{wz} = \sum_{ij} a_{wi} a_{zj} \alpha_{ij} \tag{8}$$

where the a's are the direction cosines connecting the two systems. The usual convention is to let $\alpha_{\parallel}$ be the molecular polarizability along the internuclear axis and $\alpha_{\perp}$ be the polarizability perpendicular to the internuclear axis. Then an average isotropic polarizability α and anisotropic polarizability γ are defined by:

$$\alpha = (\alpha_{\parallel} + 2\alpha_{\perp})/3 \tag{9}$$

$$\gamma = \alpha_{\parallel} - \alpha_{\perp} \tag{10}$$

The matrix elements of the induced dipole moments are then written as:

$$\langle v J M | \mu_w | v' J' M' \rangle =$$

$$\langle v J M | \sum_{ij} a_{wi} a_{zj} \alpha_{ij} E_z | v' J' M' \rangle \quad (11)$$

If we consider the vibration-rotation interaction as small, we can separate the induced dipole matrix elements into two parts; the one part containing the polarizabilities is dependent only upon the vibrational quantum numbers, while the part containing the direction cosines is dependent only upon the rotational quantum numbers.

$$\langle v J M | \sum_{ij} a_{wi} a_{zj} \alpha_{ij} E_z | v' J' M' \rangle =$$

$$\sum_{ij} \langle J M | a_{wi} a_{zj} | J' M' \rangle \langle v | \alpha_{ij} | v' \rangle E_z \quad (12)$$

Let us consider first the term dependent upon the vibrational quantum number; the matrix element in its integral form is:

$$(\alpha_{ij})_{vv'} \equiv \langle v | \alpha_{ij} | v' \rangle = \int \psi_v^*(r) \alpha_{ij}(r) \psi_{v'}(r) dr \quad (13)$$

where the ψ's are the vibrational eigenfunctions of the molecule. Now expand the polarizability in a power series in r, the relative position of the nuclei in the diatomic molecule:

$$\alpha_{ij}(r) = \alpha_{ij}|_0 + \frac{\partial \alpha_{ij}}{\partial r}\Big|_0 r + \frac{1}{2} \frac{\partial^2 \alpha_{ij}}{\partial r^2}\Big|_0 r^2 + \cdots \quad (14)$$

By substituting equation 14 in equation 13 we may find the effective terms for the various vibrational transitions. The vibrational eigenfunctions of molecular hydrogen are rigorously either even or odd functions of r. For the v = 0 to v = 0 terms (the pure rotational spectrum), therefore, only the even powers of r in the expansion of α_{ij} contribute to the matrix element, and the largest term is given by $(\alpha_{ij})_0$. For the v = 0 to v = 1 transition, the term proportional to the first derivative of the polarizability gives the largest contribution. As an approximation, the integrals may be evaluated using harmonic oscillator eigenfunctions (5, 17). Table I lists the expansion of the matrix elements and the form they take when evaluated using the harmonic oscillator eigenfunctions. Since the actual potential for the hydrogen molecule is appreciably anharmonic (9), the result is not particularly accurate. Ishiguro et al. (14) have calculated the polarizability and other similar properties of H_2, HD, and D_2 using a Morse potential function, and have pointed out the large changes in the matrix elements caused by the anharmonicity.

The part of the matrix element dependent upon the rotational quantum numbers is particularly simple, since the splitting of the M substates is too small to be observable, so that only the sum over all final M-states and the average over all initial M-states is of interest.

TABLE I

POLARIZABILITY MATRIX ELEMENTS USING HARMONIC OSCILLATOR EIGENFUNCTIONS (17)

Let $C = h/8\pi^2 \nu_e \mu c$; ν_e is the vibrational frequency for infinitesimal amplitude in cm^{-1}, and μ is the reduced mass in grams.

For $\Delta V = 0$

$$(\alpha_{ij})_{vv} = (\alpha_{ij})_0 + 1/2 \left(\frac{\partial^2 \alpha_{ij}}{\partial r^2}\right)_0 (r^2)_{vv} + \cdots$$

$$= (\alpha_{ij})_0 + 1/2\, C \left(\frac{\partial^2 \alpha_{ij}}{\partial r^2}\right)_0 (2v+1) + \cdots$$

For $\Delta v = 1$

$$(\alpha_{ij})_{v,v+1} = \left.\frac{\partial \alpha_{ij}}{\partial r}\right|_0 (r)_{v,v+1} + 1/6 \left.\frac{\partial^3 \alpha_{ij}}{\partial r^3}\right|_0 (r^3)_{v,v+1} + \cdots$$

$$= C^{1/2} \sqrt{v+1} \left(\frac{\partial \alpha_{ij}}{\partial r}\right)_0 + \frac{C^{3/2}}{2} (v+1)^{3/2} \left(\frac{\partial \alpha_{ij}^3}{\partial r}\right)_0 + \cdots$$

For $\Delta v = 2$

$$(\alpha_{ij})_{v,v+2} = 1/2 \left(\frac{\partial^2 \alpha_{ij}}{\partial r^2}\right)_0 (r^2)_{v,v+2} + \cdots$$

$$= 1/2 \left(\frac{\partial^2 \alpha_{ij}}{\partial r^2}\right)_0 C \sqrt{(v+1)(v+2)} + \cdots$$

For $\Delta v = 3$

$$(\alpha_{ij})_{v,v+3} = 1/6 \left(\frac{\partial^3 \alpha_{ij}}{\partial r^3}\right) (r^2)_{v,v+3} + \cdots$$

$$= 1/6 \left(\frac{\partial^3 \alpha_{ij}}{\partial r^3}\right)_0 C^{3/2} \sqrt{(v+1)(v+2)(v+3)} + \cdots$$

The results of the calculation are given in Table II, where $(S_J^{\Delta J})_{\parallel \text{or} \perp}^{vv'}$ is the line strength and is defined as:

$$(S_J^{\Delta J})_{\parallel \text{or} \perp}^{vv'} = \frac{1}{2J+1} \sum_{M'} \sum_{M=-J}^{+J} |\langle vJM | \alpha'_{wz} | v'J'M' \rangle|^2 \quad (17)$$

The perpendicular or parallel subscript refers to the electric vector of the light, being either perpendicular or parallel to the static electric field.

The integrated absorption coefficient $(K_J^{\Delta J})_{\parallel \text{or} \perp}^{vv'}$ is then given by:

$$(K_J^{\Delta J})_{\parallel \text{or} \perp}^{vv'} = \frac{8\pi^3}{hc} N f_{vJ} E^2 \nu_{vJ}^{v'(J+\Delta J)} (S_J^{\Delta J})_{\parallel \text{or} \perp}^{vv'} \quad (18)$$

The experimentally measured quantity is the product of the path length and the integrated absorption coefficient (see equation 3) which was denoted by A:

$$(A_J^{\Delta J})_{\parallel \text{or} \perp}^{vv'} = (K_J^{\Delta J})_{\parallel \text{or} \perp}^{vv'} \cdot L \quad (19)$$

Expressing the parameters of the right-hand side of equation 19 in laboratory units, the working relation for the absorption strength, A, is:

$$(A_J^{\Delta J})_{\parallel \text{or} \perp}^{vv'} = \frac{LPE^2}{T} f_{vJ} \nu_{vJ}^{v'(J+\Delta J)} (S_J^{\Delta J})_{\parallel \text{or} \perp}^{vv'} \cdot 1.018 \times 10^{+35} \quad (20)$$

TABLE II

THE LINE STRENGTHS

Q Branch

$$(S_J^0)_{\parallel}^{v v'} = (\alpha_{v v'})^2 + \frac{4}{45} \frac{J(J+1)}{(2J-1)(2J+3)} (\gamma_{v v'})^2$$

$$(S_J^0)_{\perp}^{v v'} = \frac{1}{15} \frac{J(J+1)}{(2J-1)(2J+3)} (\gamma_{v v'})^2$$

S Branch

$$(S_J^{+2})_{\parallel}^{v v'} = \frac{2}{15} \frac{(J+1)(J+2)}{(2J+3)(2J+1)} (\gamma_{v v'})^2$$

$$(S_J^{+2})_{\perp}^{v v'} = \frac{1}{10} \frac{(J+1)(J+2}{(2J+3)(2J+1} (\gamma_{v v'})^2$$

O Branch

$$(S_J^{-2})_{\parallel}^{v v'} = \frac{2}{15} \frac{J(J-1)}{(2J-1)(2J+1)} (\gamma_{v v'})^2$$

$$(S_J^{-2})_{\perp}^{v v'} = \frac{1}{10} \frac{J(J-1)}{(2J-1)(2J+1)} (\gamma_{v v'})^2$$

where P is the pressure in atmospheres;

L, the path length in cm;

E, the electric field in volts/cm;

T, the temperature in °K;

ν, the frequency in cm^{-1};

S is in units of cm^6;

and the other quantities were defined previously. The units of A are cm^{-1} and perpendicular or parallel refers to the orientation of the electric field vector of the light with respect to the static electric field.

The line strengths defined in equation 17 are the same as those occurring in the Raman effect (5, 18). The polarizabilities α_{01} and γ_{01} may be evaluated by the combination of Raman data and other data, as absolute Raman intensity measurements are not feasible. The ratio of the Raman intensity (v = 0, v' = 1) to the Rayleigh intensity (v = 0, v' = 0), using unpolarized incident light and collecting both perpendicular and parallel components in the transverse direction, is given by (17):

$$\frac{I_{Raman}}{I_{Rayleigh}} = \frac{(\nu-\nu_0)^4}{\nu^4} \quad \frac{45\,\alpha_{01}^2 + 13\,\gamma_{01}^2}{45\,\alpha_{00}^2 + 13\,\gamma_{00}^2} \qquad (21)$$

Secondly, the depolarization factors ρ are measured to obtain the ratios of $\frac{\alpha_{01}}{\gamma_{01}}$ and $\frac{\alpha_{00}}{\gamma_{00}}$ from the following relations (19, 20, 21):

$$\rho_{Raman} = \frac{6\,\gamma_{01}^2}{45\,\alpha_{01}^2 + 7\,\gamma_{01}^2} \tag{22}$$

$$\rho_{Rayleigh} = \frac{6\,\gamma_{00}^2}{45\,\alpha_{00}^2 + 7\,\gamma_{00}^2} \tag{23}$$

The value for α_{00} is calculated from either the dielectric constant ϵ or the index of refraction (22) of H_2 and D_2 using the Clausius-Massotti relation:

$$\frac{\epsilon - 1}{\epsilon + 2} = \frac{4\pi\,\alpha_{00} N}{3} \tag{24}$$

in which N is the number of molecules per unit volume.

2.2 Energy levels

The vibrational-rotational levels for the transitions that were observed are expressed by this equation (16):

$$T(v,J) = G(v) + F_v(J) \tag{25}$$

where

$$G(v) = \omega_e(v+\tfrac{1}{2}) - \omega_e x_e (v+\tfrac{1}{2})^2 + \omega_e y_e (v+\tfrac{1}{2})^3 + \cdots \tag{26}$$

$$F(J) = B_v J(J+1) - D_v J^2(J+1)^2 + H_v J^3 (J+1)^3 + \cdots \tag{27}$$

$$B_v = B_e - \alpha_e(v+\tfrac{1}{2}) + \gamma_e (v+\tfrac{1}{2})^2 + \cdots \tag{28}$$

$$D_v = D_e + \beta_e(v+1/2) + \delta_e(v+1/2)^2 + \cdots \quad (29)$$

Since H_v is very small, Stoicheff (9) assumed that:

$$H_v \approx He \approx H_o \quad (30)$$

The selection rules for the transitions observed in the homonuclear diatomic molecules are $\Delta J = 0$ (Q branch), $\Delta J = 2$ (S branch), and $\Delta J = -2$ (O branch), and $\Delta V = 1, 2, \ldots$

The Q branch transitions are given by the following equation:

$$Q_v(J) = \nu_{o-v} + (B_v - B_o)\,J(J+1) - (D_v - D_o)J^2(J+1)^2 \quad (31)$$

The S branch transitions are given as:

$$\begin{aligned} S_v(J) &= \nu_{o-v} + B_v(J+2)(J+3) - B_o\,J(J+1) \\ &\quad - D_v\,(J+2)^2\,(J+3)^2 + D_o\,J^2(J+1)^2 \\ &\quad + H_o\left[(J+2)^3\,(J+3)^3 - J^3(J+1)^3\right] \end{aligned} \quad (32)$$

and the O branch as:

$$\begin{aligned} O_v(J) &= \nu_{o-v} + B_v\,(J-2)(J-1) - B_o\,J(J+1) \\ &\quad - D_v(J-2)^2\,(J-1)^2 + D_o\,J^2(J+1)^2 \\ &\quad + H_o\left[(J-2)^3\,(J-1)^3 - J^3(J+1)^3\right] \end{aligned} \quad (33)$$

The best available values for the constants of H_2 and D_2 are given by Stoicheff (9) from Raman spectra measurement, but for H_2 also using Herzberg's quadrupole absorption spectra (12) for the overtones. His values were used to calculate the expected line positions.

III. THE EXPERIMENTAL ARRANGEMENT

3.1 Introduction

A block diagram of the experimental arrangement is shown in Figure 1. Continuous radiation from tungsten filament projection lamp for wave lengths shorter than 2.7μ or a Nernst glower for wave lengths beyond 2.7μ, is magnified to f/45 and focused into a light-guide type Stark cell containing the gas, then is demagnified to f/15 to match the entrance aperture of the spectrometer. After being dispersed by the spectrometer, the light is demagnified by a factor of two by a spherical mirror and is further reduced by a factor of five by an off-axis ellipsoidal mirror onto the lead sulfide photoconductive detector which could be cooled to dry ice or liquid air temperatures.

The output signal from the PbS detector is amplified by a tuned amplifier and is rectified synchronously with a reference signal derived from a mechanical chopper interrupting the beam at 90 cps for normal operation, or from a 90 cps high-voltage square-wave generator in the field-induced spectra method. The infrared signal is then recorded on a two-pen recorder, the other pen being

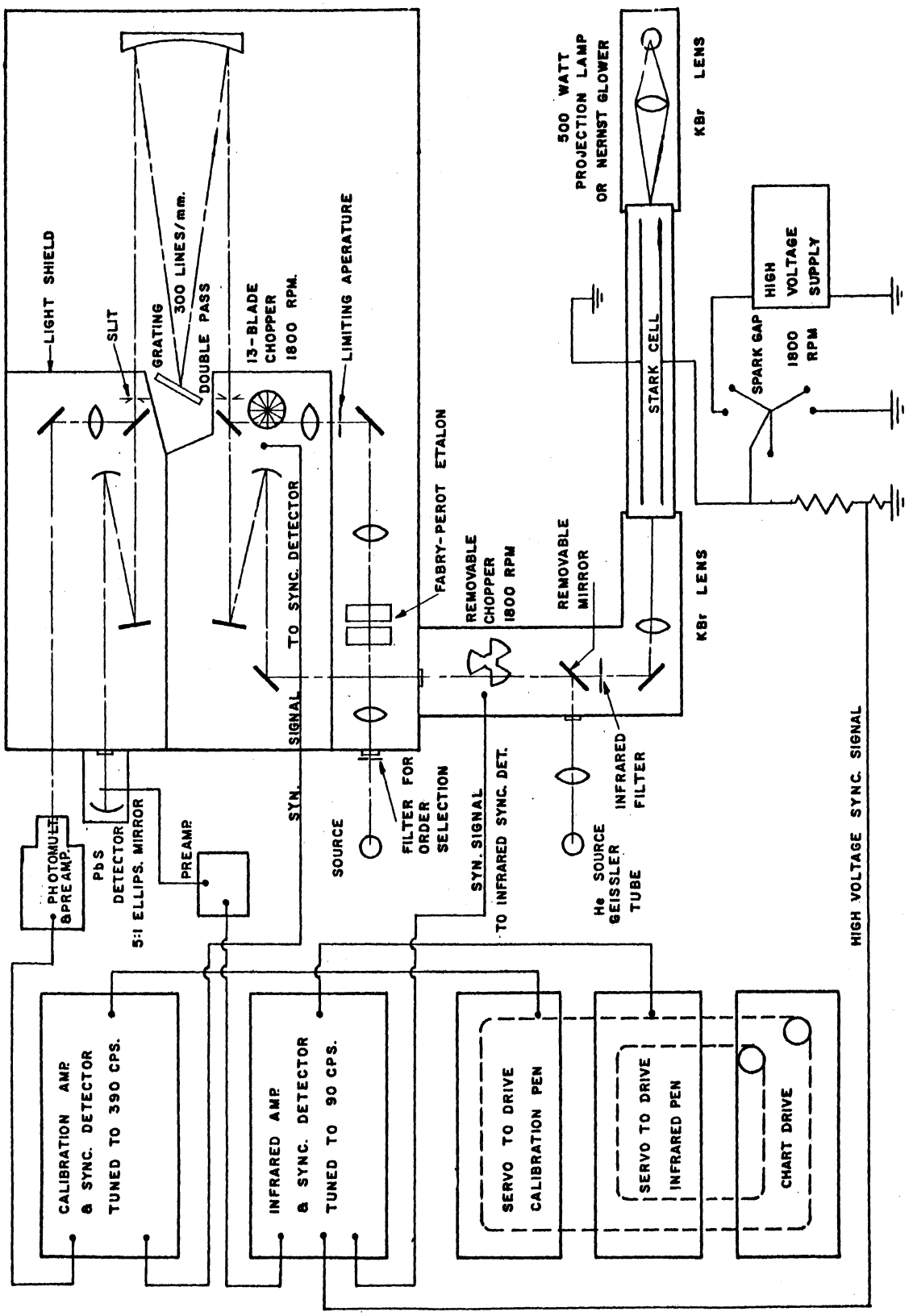

Fig. 1. Block diagram of equipment.

used to record simultaneously the fringes from a Fabry-Perot etalon calibration system.

The entire light path may be either evacuated or flushed with dry nitrogen to avoid the absorption lines due to water vapor and carbon dioxide. Evacuating the spectrometer allowed vacuum wave lengths to be measured directly, avoiding any errors due to uncertainty in the refractive index of the air.

As the electric field-induced spectra are dependent upon the direction of polarization of the light with respect to the electric field, provisions were made for measuring the polarization of the infrared radiation. A Perkin-Elmer AgCl polarizer inserted at the entrance to the Stark cell was used for wave lengths beyond 2.5μ, while Polaroid HR polarizers were used for the shorter wave lengths. The latter were inserted into the beam near the focus just before the infrared filter. A switch on the grating drive generated reference marks on the recorder traces of both channels. These pips were about 0.3 cm^{-1} apart at 4,000 cm^{-1}, and were used to record the counter number and thereby the grating angle.

3.2 The gas cell

The high-pressure gas cell is shown in Figure 2. It functions as a light guide, with the two electrodes serving as two sides and

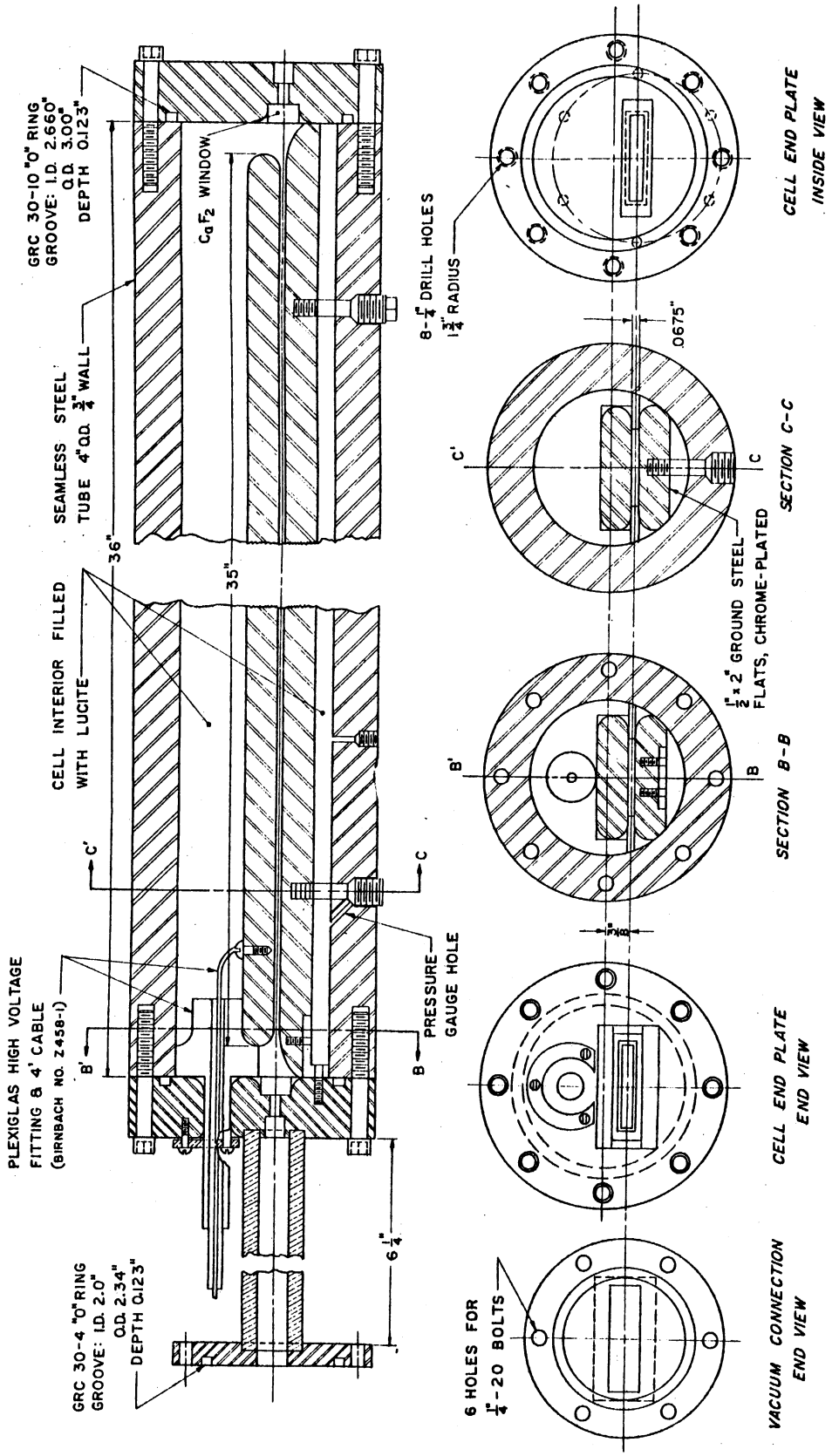

Fig. 2. High-pressure Stark effect gas cell.

the polished Plexiglas insulators as the other two sides of the guide. The light from the source was magnified by a factor of three to an aperture of f/45 to reduce the number of reflections from the cell walls and thereby to increase the transmission efficiency of the cell. The electrodes were chrome-plated ground-tool-steel flats, 36 inches long, 2 inches wide, and 1/2 inch thick, with the edges rounded to a 1/4 inch radius. The Plexiglas strips separating the electrodes were held in place with Ciba araldite epoxy resin cement. The spacing of the electrodes was 0.171 cm and the effective length was 88.3 cm (this is corrected for end effects). The upper limit to the field strength was set by the breakdown field for hydrogen, which increases with pressure to approximately 100,000 volts/cm at fifteen atmospheres (23), and then varies quite slowly with pressure. The corresponding maximum voltage applied to the electrodes is 17 kv. For other gases, appreciably higher fields could be used before breakdown of the gas would be encountered, but then problems associated with the insulation and switching, as well as corona, might arise.

The pressure in the cell was measured with an Ashcroft 1082A laboratory standard pressure gauge which had an accuracy of 0.25 percent.

The H_2 used throughout this work was obtained from the Bird Gas Corporation, and the D_2 from the Stuart Oxygen Company. Both contained some water vapor; this caused some difficulty in the O branch of H_2. A tank of extra-dry H_2 was obtained from the Matheson Company, but it was empty upon arrival, and another did not arrive soon enough to be used. The cell was always evacuated prior to filling.

The high-voltage connection to the cell was made by bringing the insulated cable (Birnbach 7458, rated at 40 kv) through a Plexiglas leadthrough and sealing the assembly with araldite cement. The windows were originally calcium fluoride, but one cleaved and was replaced with a lithium fluoride window that had a transmission limit at about 6μ wave length. They were also sealed in place with araldite cement. The whole assembly of electrodes, high-voltage connections, and one end plate slipped out of the gas chamber as a unit to facilitate alignment and cleaning. All sharp corners inside the cell and around the leadthrough were rounded to avoid corona and insulation breakdown. Lucite blocks were machined to fill in all excess space between the electrodes and the cylinder walls in order to reduce the quantity of gas required (the cell had a final volume of about 70 cc).

3.3 The high-voltage power supply

The high voltage (to 20 kv) required for the gas cell was supplied by a 140 watt RF type DC supply, similar to the one described by Mautner and Schade (24), and is shown in Figure 3. For the static electric field work, it was connected directly to the gas cell with a potential divider to read the applied voltage. For the modulated electric field technique, a rotating spark gap shown in Figure 4 was used to connect the cell alternately to the high voltage and then to ground at a 90 cps rate.

The RF oscillator high-voltage supply was a conventional type, rated at 35 kv at 5 ma, with an oscillation frequency of about 85 kc. The high-voltage step-up coil was obtained from Spellman Electronics, New York City. The filaments of the high-voltage rectifier were heated by a separate RF oscillator operating at about 3 megacycles per second. An RF supply avoided the special high-voltage insulation that otherwise would have been required in the filament circuit.

The gas cell had a capacitance of about 850 μμf, and required 0.17 joule to charge it to 20 kv. For a 90 cps repetition rate, the power consumption by the cell was 15 watts, which was dissipated in the charging and discharging circuit (25). Five 0.5 megohm resistors, each of six-watt capacity (25 kv rating) were placed in series with the spark gap and the cell to prevent overheating of the insulation,

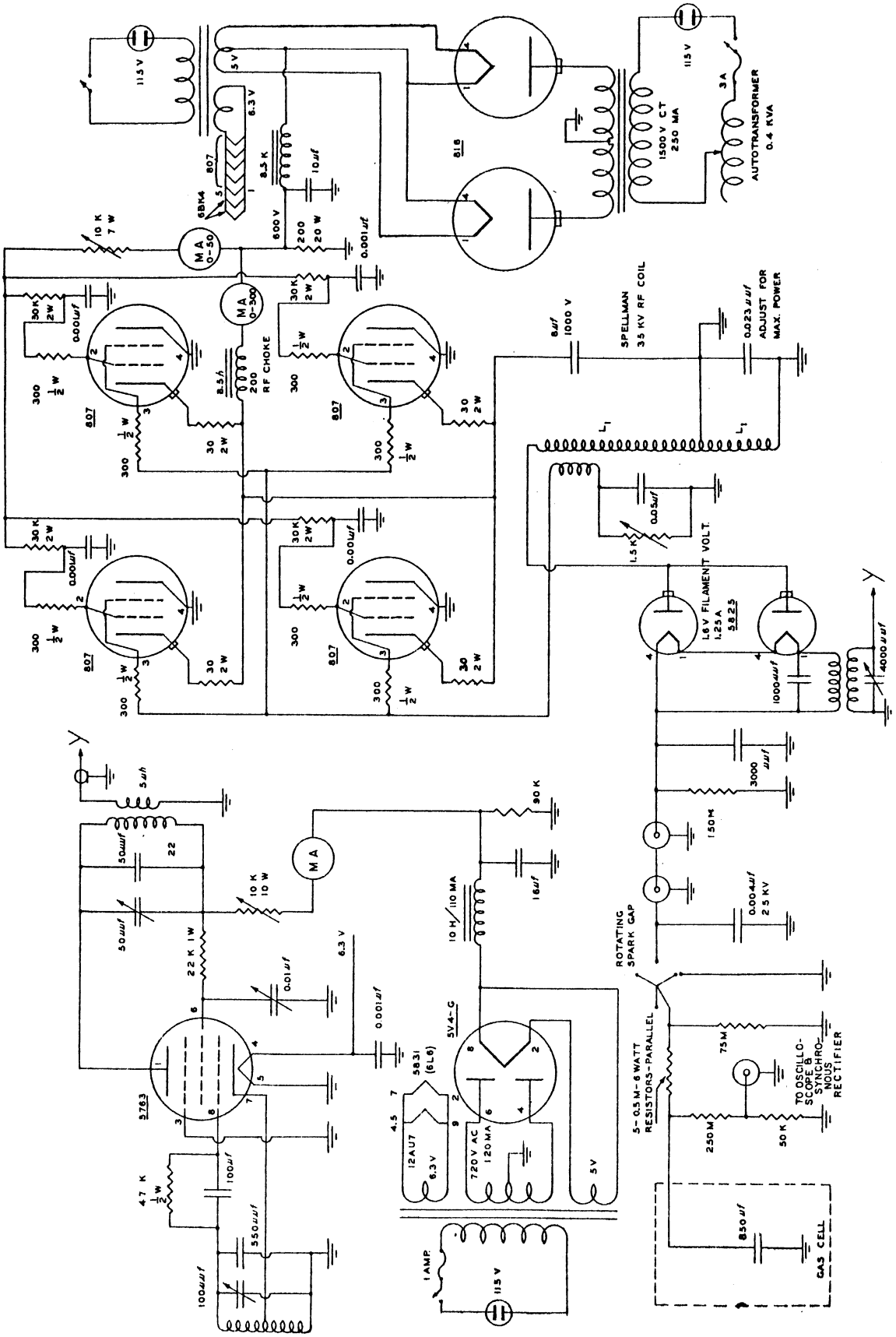

Fig. 3. High-voltage power supply.

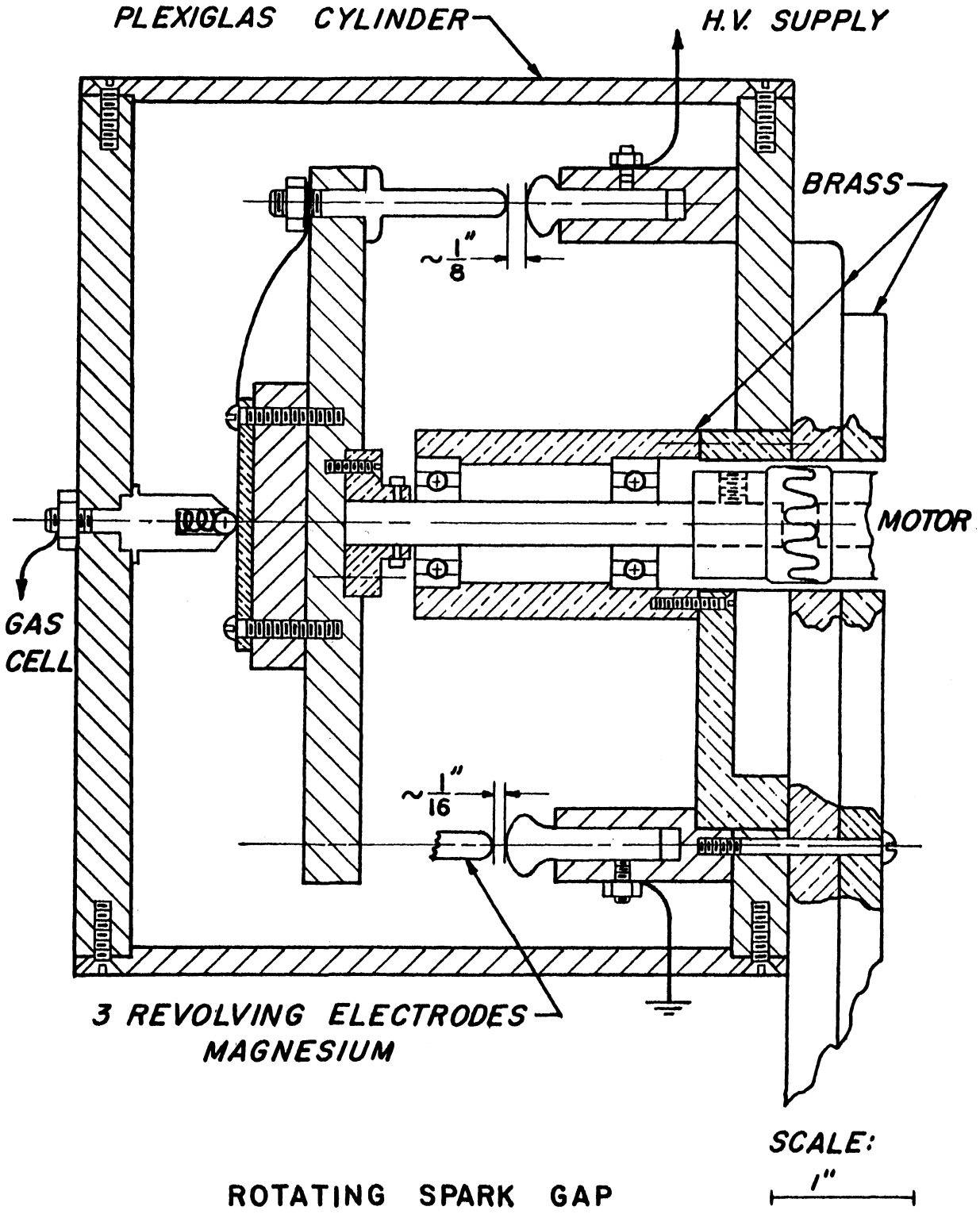

Fig. 4. Rotating spark gap.

and to reduce spark gap erosion as well as noise radiation from the spark. These resistors along with the cell capacitance gave a rise time constant of 71 microseconds, which was much less than the signal period of 11,000 microseconds.

A 0.004 μf storage or filter capacitor (large compared to the capacitance of the gas cell) was placed between the high-voltage line and ground just before the spark gap to serve as a charge ballast to insure a short time constant on charging the gas cell.

Provisions were made in the high-voltage power supply for the insertion of four 6BK4 regulator tubes. Although the supply was sufficiently stable for this work, such regulator tubes may be useful subsequently.

The rotating spark gap shown in Figure 4 was used as a high-voltage switch. The high-voltage lead to the gas cell was connected to the center fixed electrode, the high-voltage supply to the upper fixed electrode, and the ground to the lower fixed electrode. The rotating wheel had three electrodes all connected to the center fixed electrode. As the wheel was rotated at 1800 rpm by a synchronous motor, the cell was alternately switched to the high voltage and then to ground. It was found necessary to space the upper electrode about 1/8 inch from the moving electrodes to avoid a premature breakdown which produced a stepped wave form rather than the

square wave desired. The maximum voltage obtainable was reduced by the potential drop across the spark gap of the order of 1 kv.

Magnesium electrodes were used in the spark gap as they were light and self-cleaning. The mushroom shape reduced the jitter or erratic breakdown at both ends of the square pulse, and also gave greater electrode life due to the greater area.

A considerable amount of ozone was generated by the sparks and accumulated in the housing until there was sufficient vapor present to produce a mild explosion. In order to avoid this interruption in the continuity of the experiment, dry N_2 was continuously passed through the spark gap assembly.

The high-voltage signal was measured by means of a resistor potential divider consisting of a 250 megohm resistor (rated at 40 kv) and a 50,000 ohm resistor. The ratio of these was determined to be 5058 ± 0.1 percent with a Wheatstone bridge circuit. The synchronizing signal for the detection system was derived from this network also.

The wave form was actually trapezoidal due to the discharge time constant of the gas cell through the resistances to ground, and the quenching of the spark across the grounding gap. The average of the squares of the voltages was taken as the effective voltage

since the intensity of the induced absorption is proportional to the square of the field.

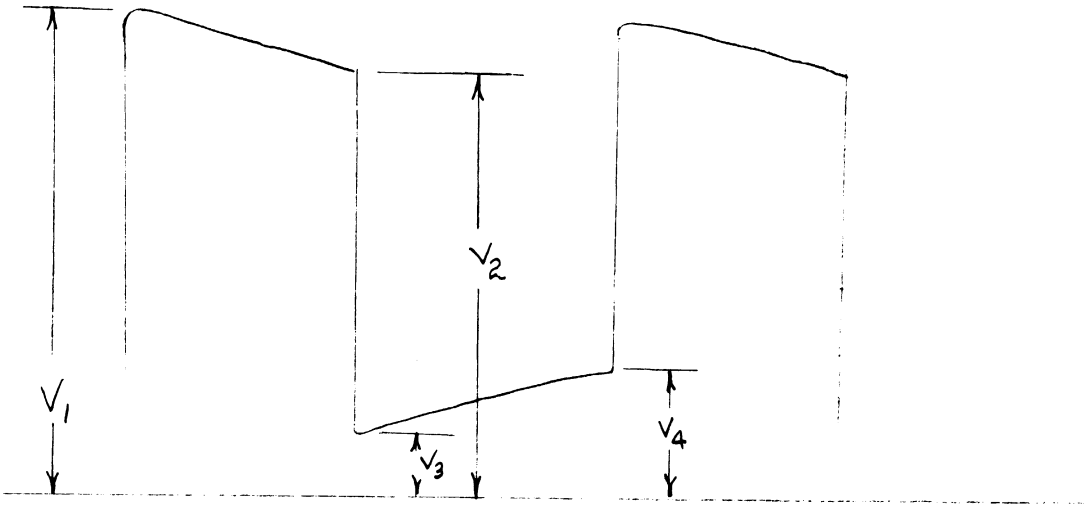

$$V_{eff} = \sqrt{\frac{V_1^2 + V_2^2}{2} - \frac{V_3^2 + V_4^2}{2}}$$

Typical values for these voltages were: V_1 = 17 kv; V_2 would be 15.3 kv; V_3 about 1.5 kv; and V_4 about 2.0 kv. The values were obtained from the face of a Dumont 304A oscilloscope using the DC amplifier in the vertical deflection channel. The vertical sweep was calibrated just prior to a run against a dry cell which had been measured previously with a precision potentiometer; the accuracy in reading the voltage from the oscilloscope face was the limit to the accuracy of the polarizability measurement.

3.4 The spectrometer

The spectrometer used in this work is the Ebert-type high-resolution vacuum grating monochromator designed and built by Marshall (26) and modified by Brown (27). The instrument has a 119 inch focal length, 24 inch diameter, spherical mirror, gold plated for high reflectivity in the near infrared.

The grating used was a Bausch and Lomb replica with a ruled area, 127 mm by 203 mm, having 3000 rulings per cm. The blaze angle was 25.6°, corresponding to about 2.8 microns in this spectrometer. The grating was double-passed (28) throughout this investigation to increase the dispersion. This had an undesirable effect in the Q branches of hydrogen which occur at angles less than the blaze angle for the first-order spectrum of the fundamental (v = 0 to 1 transition) and for the first- and second-order spectra of the first overtone (v = 0 to 2 transition). The light with the electric field parallel to the static electric field (the component that is most strongly absorbed in the Q branches by a factor of about 50) was only 25 percent of the total intensity in the Q branch region. The effect of the double passing of the grating in these regions was to double the dispersion but also to further reduce the component that would be appreciably absorbed. A 12,000 line/inch grating

blazed for two microns would not have this large polarizing effect (29) in the Q branch region, but one was not available at the time.

The theoretical resolving power R_o of a multipassed grating is the product of the number of passes, r, and the number of lines on the grating, or in this case: $R_o = \frac{\nu}{\delta\nu} = 122{,}000$. At 4000 cm^{-1}, this would lead to a theoretical spectral width $\delta\nu$ of 0.03 cm^{-1}. Brown observed a resolving power of about 100,000 or 0.04 cm^{-1} for this instrument double-passed which was commensurate with the influence of the finite half-width of the absorption lines. The pressure-broadened width of the H_2 absorption lines observed in this investigation was about 0.15 cm^{-1} for the pressures used in the gas cell. The instrument was consequently operated at spectral slit widths between 0.1 and 0.2 cm^{-1} as a compromise between detectability and resolution.

The interfering orders from the grating were eliminated by filters. For the major portion of the work, a single germanium filter transmitting only beyond 1.8 microns was sufficient. At wave lengths beyond 3 microns a Bausch and Lomb multilayer dielectric long wave length pass filter was added. In the v = 0-2 transition of H_2, which occurred at 1.2 microns and was measured in the second order, the first order was eliminated with an ammonium dihydrogen phosphate crystal which has a long wave length cutoff about 1.7

microns, and the third and higher orders with a Corning 2540 filter which only passes radiation beyond 0.9 micron. The v = 0-2 transition in D_2 at about 1.7 microns was studied in second order using a glass filter to absorb the first order, and a crystal of silicon absorbing below 1.2 microns to cut off the third and higher orders.

To locate the approximate positions in the spectrum, a grating equation was formulated in terms of the counter numbers on the rotation of the grating drive:

$$\nu = \frac{n \cdot 1503.53}{\sin [0.00223744 \ (C - Co)]}$$

where n is the spectral order; C, the counter number; and Co, the grating zero or central image. Due to a defect in the grating drive, the grating zero, Co, changed erratically and shifted the spectral positions by up to 0.2 cm^{-1}. The instrument was also found to be slightly temperature sensitive, probably because of a difference in expansion between the aluminum bedplate and the steel drive tape. A close check of the temperature during a run was maintained with a Wheatstone bridge having a thermistor in one arm. This thermistor was anchored to the bedplate in the vicinity of the grating drive mechanism. A resistance change corresponding to 0.003°C change in the bedplate could be detected. The primary calibration, however, was by means of the Fabry-Perot etalon system to be described

later so that this erratic behavior was a handicap rather than a limitation.

The pressure in the spectrometer was generally held below 50 microns of Hg. While the data were being taken, the pumps had to be turned off to stop noise arising from vibration, but the large volume of the tank provided sufficient ballast so that the pressure remained below 100 microns of Hg. The effect of the index of refraction of air at this pressure was below the accuracy of the calibration.

3.5 The exit optics and infrared detector

The exit optics of the spectrometer consisted of a spherical mirror which demagnified the exit slit image by a factor of two and an off-axis ellipsoidal mirror which reduced the image another factor of five. The ellipsoidal mirror was in the detector housing (see Figure 5) and could be adjusted without destroying the vacuum by distorting the brass bellows.

The detector was mounted on a copper rod which extended through the vacuum housing into a Dewar flask containing the coolant, either dry ice-alcohol or liquid air. The rod was mounted on thin stainless steel tubing to cut down conduction heat transfer. To reduce the radiation noise on the detector (30), a cooled radiation

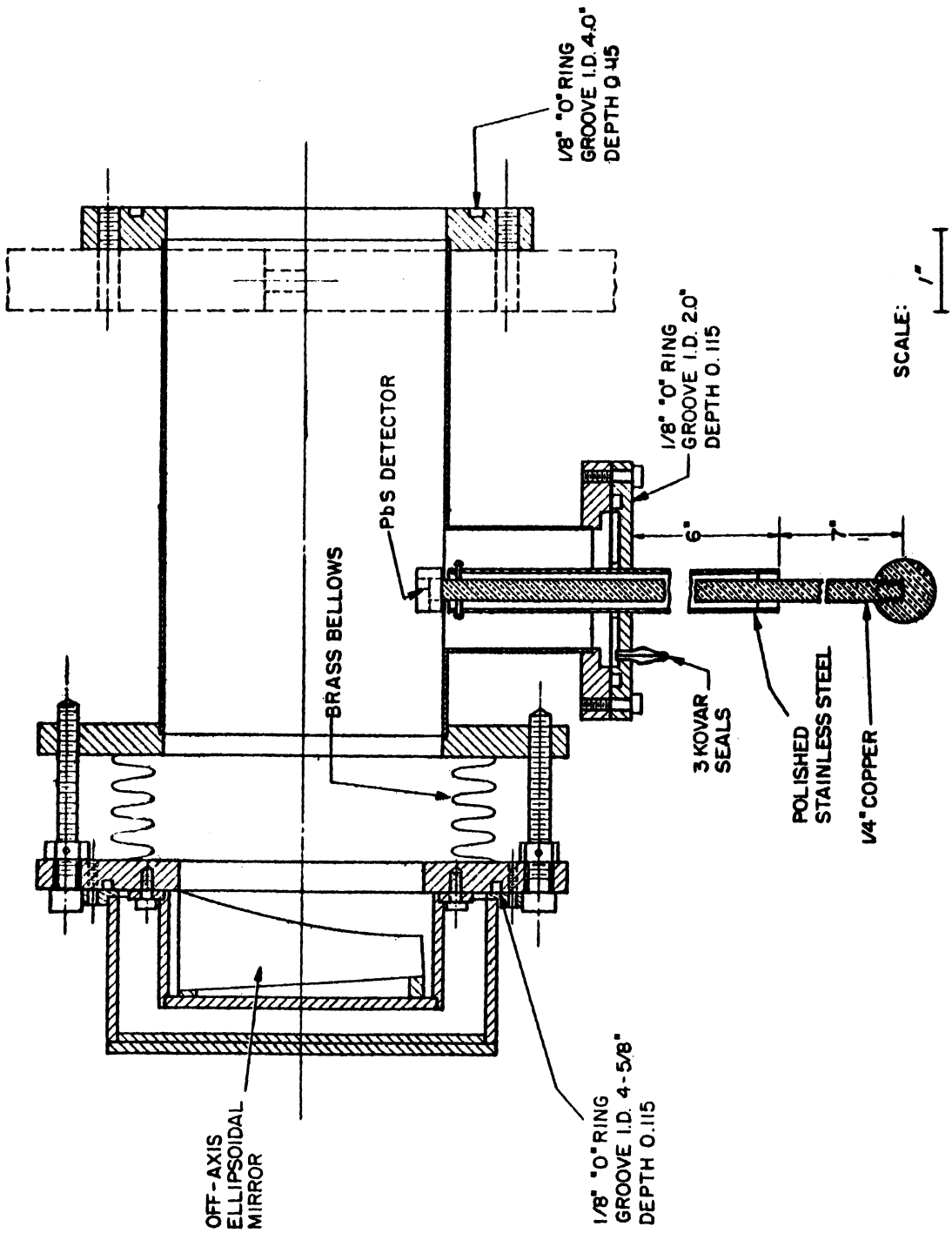

Fig. 5. Detector housing.

shield was placed around the detector, permitting it to "see" only the ellipsoidal mirror.

The infrared detectors used were Eastman Kodak Ektron lead sulfide photoconductive cells with their geometry chosen to match the exit optics as nearly as possible. The cells were 0.25 × 2.5 mm with the electrodes parallel to the long dimension. The cells were cooled to dry ice and liquid N_2 temperatures, both to increase their signal-to-noise ratio and to extend their long wave length response (23). The resistance of the lead sulfide increased with decreasing temperature, and the bias resistors in series with the cells were changed to match the resistance of the cells at the working temperatures. Table III lists the resistance and signal-to-noise data of two of the cells used--a conventional lead sulfide and a "plumbide" detector--at these temperatures. "Plumbide" is a special lead sulfide with an enhanced long wave length response. The signal-to-noise data were taken at various slit widths and with a four-second time constant. For the synchronous detector system, the time constant is related to the band pass by $\pi \Delta f S = 1$, where Δf is the band pass in cycles/sec. and S is the time constant in seconds. This was used to recompute the data for the standard 1 cycle/sec. form. The signal-to-noise varied as the square of the spectral slit width; but all of the values were recomputed using this

TABLE III

PERFORMANCE OF LEAD SULFIDE DETECTORS
IN EBERT SPECTROMETER
(tungsten filament source and germanium filter)

Detector	Resistance	Wave Length	Signal to Noise[a]
At Room Temperature			
Lead sulfide	230 K	2.0 μ	40,000
Lead sulfide	230 K	2.5 μ	25,000
Plumbide	30 K	2.5 μ	2,000
At Dry Ice Temperature			
Lead sulfide	3.3 meg	2.5 μ	130,000
Plumbide	200 K	2.0 μ	28,000
Plumbide	200 K	2.5 μ	28,000
At Liquid Air Temperature			
Lead sulfide	160 meg	2.5 μ	300,000
Plumbide	3 meg	2.0 μ	150,000
Plumbide	3 meg.	2.5 μ	150,000
Plumbide	3 meg.	3.15μ	50,000
Plumbide	3 meg	3.34μ	11,000

[a] Corrected to 1 cm^{-1} spectral band pass and 1 cycle/sec. amplifier band pass.

relation for a 1 cm^{-1} spectral slit width. The noise is one-quarter the peak-to-peak excursions of the pen (excluding the random infrequent large swing). The long wave length data with the Nernst glower source was representative of that used in the D_2 work.

Cooling the lead sulfide cells turned out to be somewhat of a risk, particularly with liquid nitrogen. The contraction due to the temperature change not infrequently caused the soldered electrode to separate from the rest of the detector, in which case a new detector had to be installed. The detectors of one type varied quite a bit in sensitivity as well as spectral response, so that a broken detector was a minor calamity.

The important detector characteristics for low-level electric field-induced spectra work are the dynamic range (the ratio of maximum signal without cell saturation to the noise) and the linearity of the cell response. The former was not studied in detail since at the slit widths used not enough radiant power was transmitted to saturate the cell. The lead sulfide detector, both at dry ice and liquid N_2 temperatures, did saturate at signal-to-noise ratios of about 3000 for a 1 cycle bandpass. The dynamic range of the plumbide detector at liquid N_2 temperature appeared to be about 8000 for 1 cycle bandpass. The dynamic range of the detector determined the smallest value of the modulated absorption that could

be detected. In general, the dynamic range appeared to be much greater for detectors at room temperature. The linearity characteristic is important for accurate intensity measurements, although it is of no particular concern in determining line positions. The detectors were found to be linear over a very wide range nearly to saturation. The linearity was tested in a variety of ways: (a) by a neon bulb flashed at 90 cps in a strong DC light beam that was varied; (b) by varying the source intensity and observing the change in the intensity of electric field-induced absorption; and (c) by inserting filters and polarizers into the beam so as to vary the background signal but with only known minor changes (reflection losses, et cetera) in the electric field-induced absorption signal. Throughout the dynamic range of the detector, the linearity was found to hold within experimental error in all cases.

3.6 The calibration system

The calibration system utilized white light Fabry-Perot fringes that were recorded simultaneously with the infrared spectra (27), similar to the work of Douglas and Sharma (31) and Plyler et al. (32).

A tungsten filament projection lamp was used as the source of radiation. An achromatic lens collimated the light onto the Fabry-Perot etalon with a second identical lens forming the image on a

variable auxiliary aperture that isolated the central fringe. The image was then magnified by a factor of two to match the entrance solid-angle aperture of the spectrometer. The image from the Fabry-Perot etalon was placed low on the entrance slit below the infrared beam and after being single-passed through the spectrometer was received at the upper end of the exit slit. A lens system then focused this light onto a Dumont 6292 photomultiplier placed outside the vacuum tank of the spectrometer. By proper choice of the Corning glass filters (33) in conjunction with the long wave length cutoff of the photomultiplier at 0.62μ; grating orders other than the one desired could be rejected.

The white-light Fabry-Perot system forms a set of fringes equally spaced on a wave-number scale which may be recorded simultaneously with the infrared spectrum on a two-pen recorder. For the interferometer in a vacuum (in this case the spectrometer), the spacing of the fringes is dependent only upon the interferometer spacing, t. The spacer separating the quartz interferometer plates was made of invar in order to keep the effect of temperature variation to a minimum. The maximum drift during a run was about 0.02 cm^{-1} but was usually much less.

The interferometer equation is:

$$\frac{m}{\nu} = 2t \cos \phi \qquad (34)$$

where m is the order number, ν is the frequency in cm^{-1}, and ϕ is the angle between the ray and the normal to the interferometer surfaces. The interferometer was carefully aligned so that ϕ was 0, and hence:

$$\nu_v = m K \tag{35}$$

where K is the etalon constant in cm^{-1} and is equal to $\frac{1}{2t}$. The visible light passing through the etalon corresponds to a certain frequency ν_I of the infrared where the visible light is given as

$$\nu_v = \frac{n_v C}{\sin \theta} \tag{36}$$

and the infrared light as

$$\nu_I = \frac{n_I C}{\sin \theta} \tag{37}$$

where C is the grating constant; θ, the grating angle; n_I, the spectral order of the grating for the infrared radiation; and n_v the grating spectral order of the visible light through the Fabry-Perot interferometer.

Hence:

$$\nu_I = m \left(\frac{n_I}{n_v} K \right) \tag{38}$$

where the quantity in parentheses is the effective etalon constant.

The infrared spectral order was determined by the filters used in the infrared channel, and the visible spectral order by the combination of filters and photomultiplier cutoff in the interferometer channel. The quantity m will then describe a frequency of light ν_I for a given etalon constant.

To determine the etalon constant initially, the number of fringes between two lines of known frequencies, ν_1 and ν_2, were measured. This same method was then used to determine the frequency difference between a known line and the line being measured.

The quality of the Fabry-Perot fringes, the ratio of Intensity_{max} to Intensity_{min}, varied with the size of the exit slit which acted as the scanning aperture. The quality of the fringes is very dependent upon the size of this aperture (34). Table IV gives some fringe qualities that were obtained with the calibration system under different conditions of etalon spacing, slit width, and auxiliary aperture. At 4000 cm^{-1}, 25-micron-width slits were equivalent to a spectral width of about 0.04 cm^{-1}; 50-micron slits to 0.05 cm^{-1}; and 100-micron slits to 0.08 cm^{-1}. Above 100 microns, the spectral width varied linearly with slit width.

In this investigation, the etalon was initially calibrated using the 1.0829 micron helium line in second order and the R(19) and P(20) lines of the first overtone of CO. All lay in the region where

TABLE IV

FABRY-PEROT FRINGE QUALITY
(at 4000 cm^{-1})

Slit Width	Aperture	$\frac{I_{max}}{I_{min}}$	Width at Half Ht. / Width of Order
	For 5 mm Spacer, Fourth Order on Grating		
50 μ	1/16"	52/48	
25 μ	1/4"	60/45	
25 μ	1/8"	48/32	
25 μ	1/16"	31/18	
	For 2 mm Spacer, Fourth Order on Grating		
250 μ	1/8"	90/72	
150 μ	1/8"	100/45	0.46
100 μ	1/8"	87/25	
50 μ	1/8"	70/12	
25 μ	1/8"	94/13	0.35
	For 1 mm Spacer, Fourth Order on Grating		
250 μ	1/4"	80/33	0.45
150 μ	1/4"	78/19	0.41

visible light of the fringe system was in the fourth spectral order of the grating. The helium line had been measured photographically with an interferometer by Meggers and Humphreys (35). Their value for the wave length in air which is accurate to about one part in 10^7 was corrected to vacuum wave lengths using the refractive index data of Edlen (36). (The correction of Rank et al. [37] to Edlen's formula would be about three parts in 10^7 which is beyond our present calibration accuracy.) The CO lines had been measured interferometrically by Rank et al. (38) to an absolute accuracy of about two parts in 10^7.

The value of the etalon obtained from the initial calibration was used in conjunction with the P(19) line to obtain the frequency of the $Q_1(0)$ electric field-induced absorption line of H_2; the two lines are only about 14 cm^{-1} apart. The position of the $Q_1(0)$ line in combination with the He line was used in all subsequent H_2 measurements. The S lines of H_2 were measured relative to the second order He line. In D_2, the etalon constant measured from the H_2 work was used to calculate the Q branch lines relative to the third order of the 1.0829 micron He line as this was less than 100 cm^{-1} from the Q branch.

The S branch lines of D_2 were measured relative to the fifth order of the 0.5875 micron and the fourth order of the 0.7065 micron

lines of He; the former was about 15 cm^{-1} from the S(2) line and the latter was near the S(5) lines of D_2. The wave lengths of these lines were taken from Crosswhite and Dieke (39).

Temperature fluctuations in the spectrometer set the limit on the accuracy of the measurements which is estimated to be ± 0.02 cm^{-1}. During a run, the spectrometer bedplate was monitored continuously to insure the correct etalon calibration.

The vacuum tank of the spectrometer was used as the gas cell for the carbon monoxide as the optical path length for the double-passed beam was about 86 feet and pressures as low as 300μ Hg could be used which avoided pressure broadening the absorption lines.

The helium lines were excited in a Geissler tube by a 5 kv neon-sign transformer. The beam was brought into the infrared channel through a right-angle prism that slipped into the beam in the foreoptics.

3.7 The electronic detection system

The infrared channel and the calibration channel used the tuned amplifier-synchronous rectifier technique, similar to that of Hickmott and Terhune (40). In normal operation, the infrared channel was modulated at 90 cps by a three-bladed light chopper driven

by an 1800 rpm synchronous motor; the blade also chopped a light beam incident on a phototube, producing the synchronizing signal. In recording the electric field-induced spectra, the high-voltage electric field inducing the absorption produced the synchronizing signal through a voltage divider network. This was also a 90 cps rate set by the rotating spark gap.

The calibration channel was modulated at 390 cps using a thirteen-bladed chopper on an 1800 rpm synchronous motor. This chopper also modulated the input to a phototube, providing the synchronizing signal for the calibration channel. The chopping frequencies were chosen so as to avoid cross talk with the 60 cps line and between each other. Synchronous drives were mandatory to prevent beating with the line frequency.

The infrared amplifier and the calibration amplifier used the AC coupled high-gain cascade triode circuit devised by Wylie (41) with the addition of negative feedback for stability and linearity. Band-pass LC filters were used to eliminate the third and higher harmonics that arise in the square-wave modulation because the synchronous rectifier system does not reject odd harmonics. Daven attenuators (1.5 db per step) were used in both amplifiers to adjust the gain.

The synchronous rectifiers (the infrared synchronous rectifier is shown in Figure 6) had electrical phase shift adjustments to obtain the proper phase relations between the synchronizing signal and the signal carrying the information. The phase was adjusted for maximum deflection of the recorder with an infrared signal input for the normal mode of infrared operation and for a known spectral line in the electric field-induced method. The phase could also be adjusted by monitoring the Lissajou figure from the mid-point and one arm of the synchronous rectifier bridge. (The points are labeled upper and left in Figure 6.) When the signals were out of phase, the signal was a figure eight, very full, and was a "V" when they were in phase. This was a good check of the phase relations for either type of operation.

Both preamplifiers were RC coupled using triodes. The first stage of the infrared preamplifier employed a 6CB6 connected as a triode and operated at a reduced plate supply voltage to reduce tube noise (42). The infrared preamplifier had an additional attenuator switch of a factor of eight after the first stage to prevent high-level signals from overloading any succeeding stage.

The noise from the first stage of the infrared preamplifier was the predominant noise in the circuit, and it in turn was down by a factor of three or more from the current noise of the lead

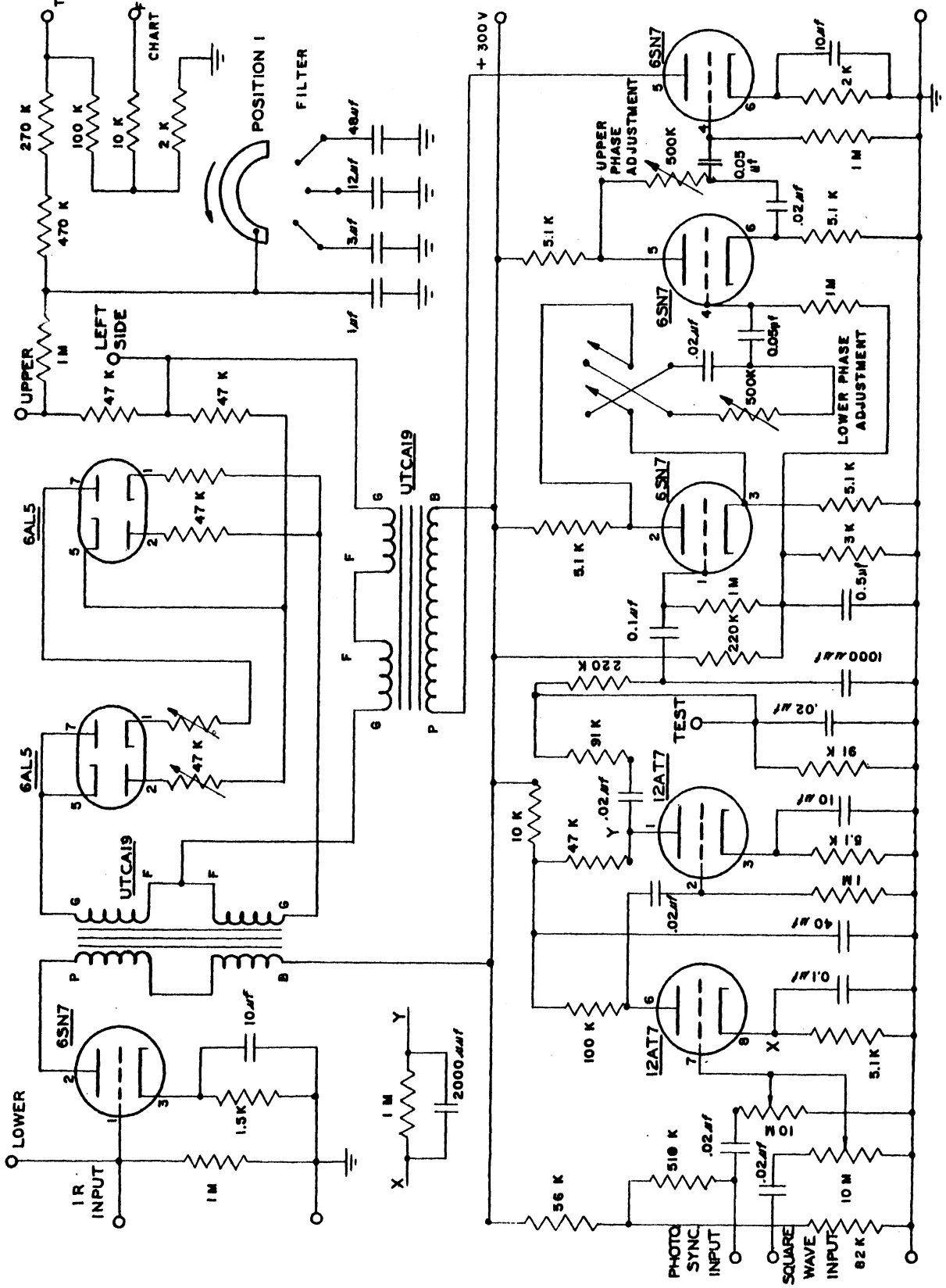

Fig. 6. Infrared synchronous rectifier.

sulfide detector. The high-voltage spark gap would only cause excess noise (of a very erratic variety) when there was a poor connection in a lead to the first tube, especially corrosion in the connector in the lead between the detector and the grid of the first stage, or there was a portion of the circuit that was not adequately grounded. In general, the entire electronics system had to be "cleaned up" to a very high degree to permit operation of the high-voltage spark gap without an increase in the noise level.

IV. RESULTS AND CONCLUSIONS

4.1 General results

The high detectability of induced infrared absorption of H_2 and D_2 with this particular apparatus is illustrated by the rapidly scanned traces of the Q branches of each molecule reproduced on Figures 7 and 8. The experimental conditions are given in the legend with each figure--the most noteworthy being the spectral band width of 0.2 cm^{-1} for H_2 and 0.1 cm^{-1} for D_2. This resolution is the equal of that of the best available Raman spectra, but the signal-to-noise level is vastly increased. The lower signal-to-noise ratio in the D_2 spectrum near 3000 cm^{-1} is due to the dwindling response of the lead sulfide detector whose long wave length limit of sensitivity is not far beyond 3000 cm^{-1}. This situation made it impossible to observe any Q lines of D_2 having J larger than 4.

The absorption strength of the lines, as expressed in equation (20), was observed to vary linearly with the pressure of H_2 in the cell, but quadratically with the electric field intensity across the cell. Both dependences are to be expected from the theory. The

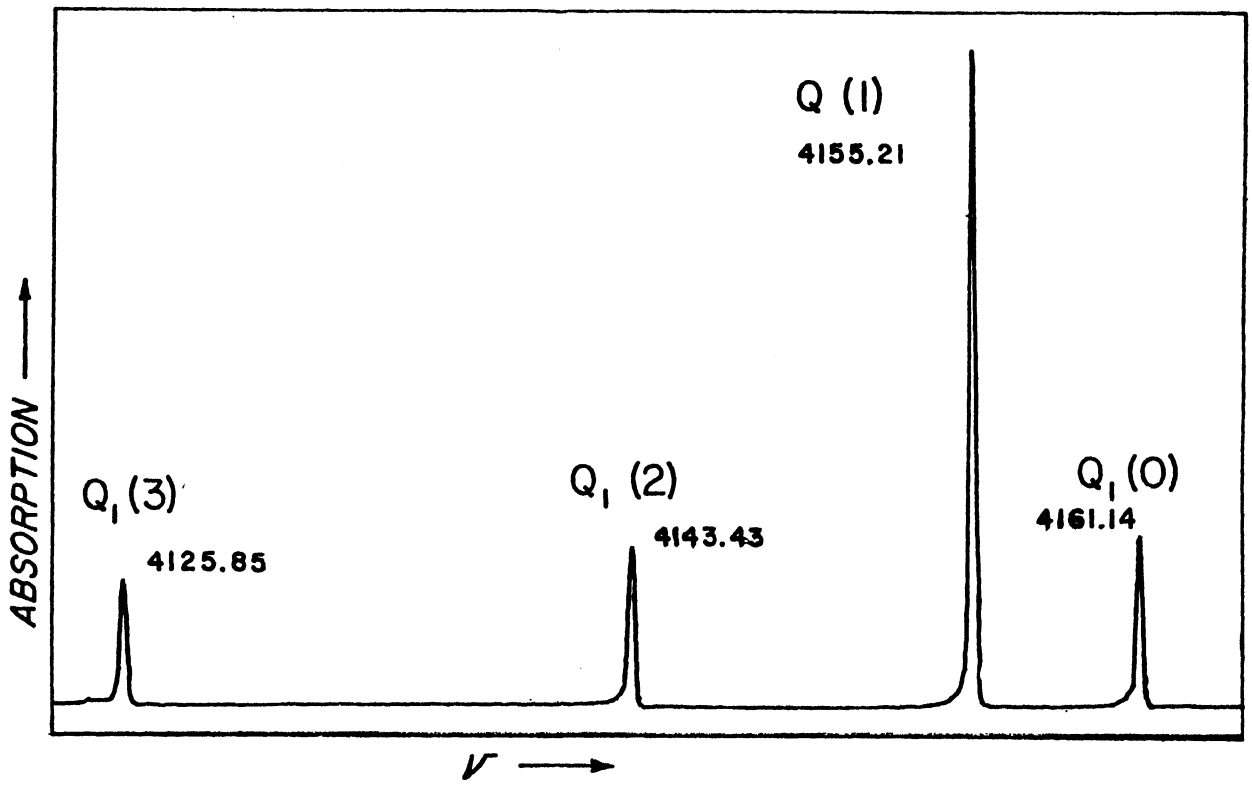

Fig. 7. Q branch of ν_{0-1} of H_2. 87,000 volts/cm, 21.5 atm of H_2, 1-sec response, 0.2 cm^{-1} slits.

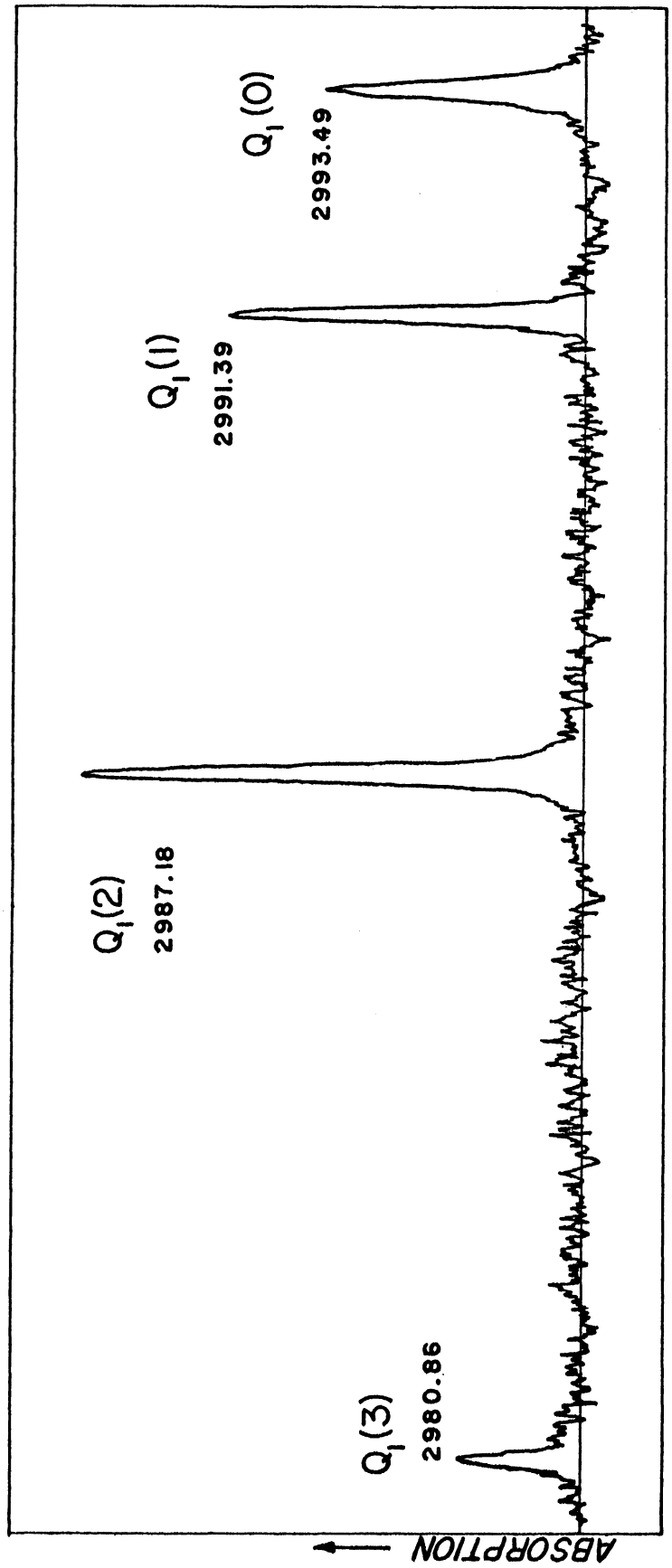

Fig. 8. Q branch of $\nu_{0\text{-}1}$ of D_2. 87,000 volts/cm, 21.5 atm of D_2, 4-sec response, 0.1 cm^{-1} slits.

accuracy of both measurements was set by the uncertainty in the value of the electric field strength (± 3 percent).

Although the induced absorption increases with the pressure, the optimum pressure is dependent upon two additional factors (considering the cell length fixed). Pressure- or collision-induced absorption also occurs and gives rise to a broad, continuous absorption chiefly in the region of the fundamental (42). This absorption is proportional to the square of the pressure and leads to a reduced signal at high pressures. It is not modulated by the AC electric field in the cell, however, and hence only reduces the amount of flux falling on the detector. In the overtone region either extremely high pressures or very long cells could be used before there would be an appreciable pressure-induced background.

The second factor influencing the choice of pressure concerns the pressure dependence of the width of the absorption lines. This factor sets the limit on the accuracy of the measurements of the line positions. Data were taken on the line width of $Q_1(0)$ of H_2 using slit widths to give a 0.10 cm^{-1} spectral band pass (demonstrated by the line widths of the overtone of CO at very low pressure). The values obtained were 0.16 cm^{-1} half-width at 250 psi and 0.21 cm^{-1} at 500 psi. Additionally, it was found that the line

width was independent of the electric field strength up to values of 100,000 volts/cm^{-1}.

In view of these results, actual operating conditions for most of the work were set by using the highest electric field strength that could be maintained constant by the high-voltage power supply (100,000 volts/cm max), and a pressure high enough to prevent breakdown in the cell (fifteen atmospheres was adequate). In the case of very weak lines, the pressure was increased to a maximum of thirty-five atmospheres. Wherever possible, spectral slit widths slightly smaller than the line widths were used (usually 0.15 cm^{-1}), but again the very weak lines could only be detected with wider slits.

Some measurements were taken with a static electric field on the Q_1 lines of H_2 to check the accuracy of the intensity values obtained with the 90 cps square-wave field, and the results agreed within the estimated error. All subsequent data were taken with the modulated-field method, and the majority of the lines were so weakly absorbing that they could only be detected in this fashion.

Some typical traces of the electric field-induced spectral lines of H_2 are presented in Figures 9 through 13, and of D_2 in Figures 14 through 16. In order to obtain the relative strengths of the various lines, these traces had to be corrected for the relative gain of the amplifier, the detector sensitivity, and the polarizing effect of the

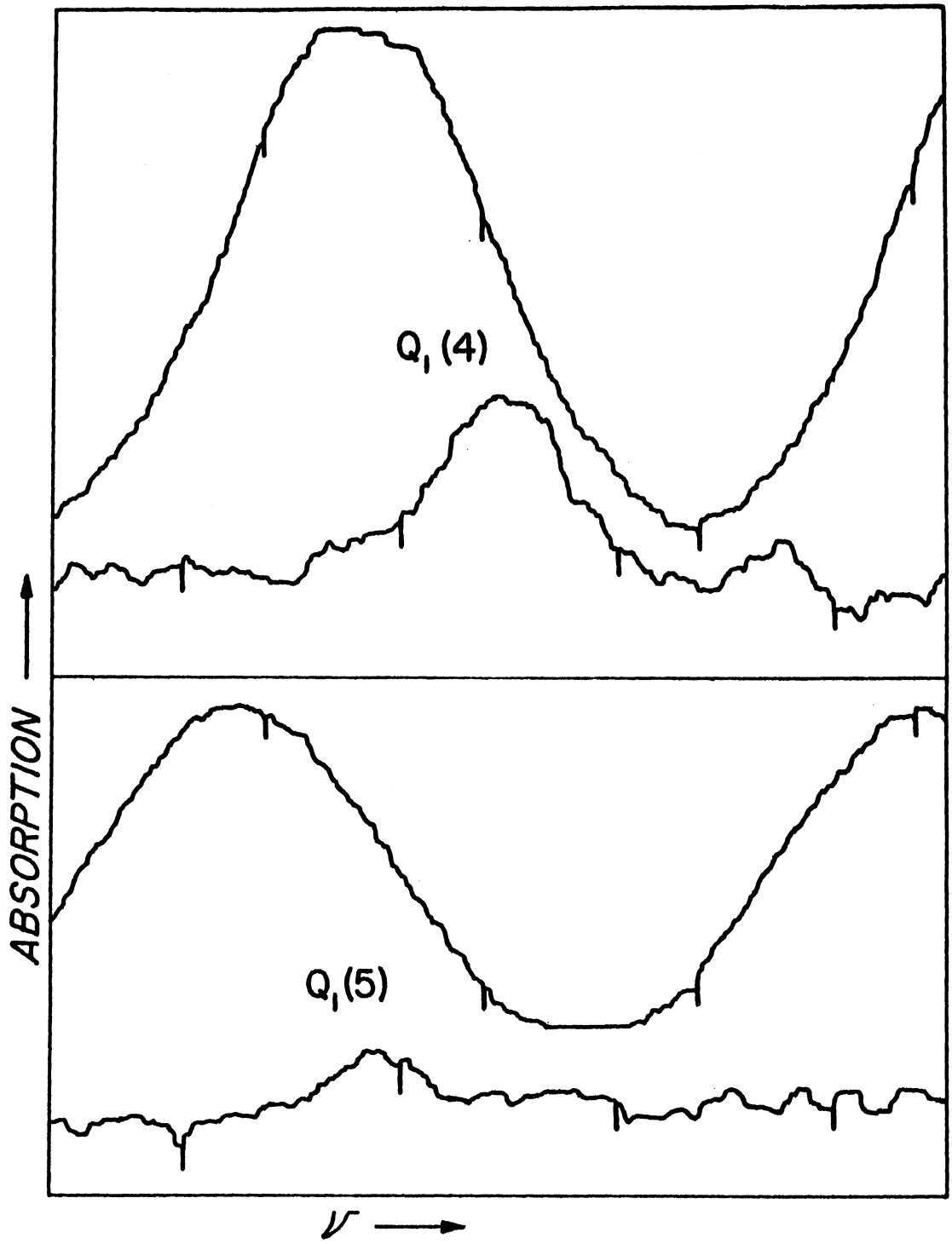

Fig. 9. $Q_1(4)$ and $Q_1(5)$ of ν_{0-1} of H_2. 88,000 volts/cm, 21 atm of H_2, 16-sec response, 0.2 cm^{-1} slits, fringe spacing 1.25 cm^{-1}.

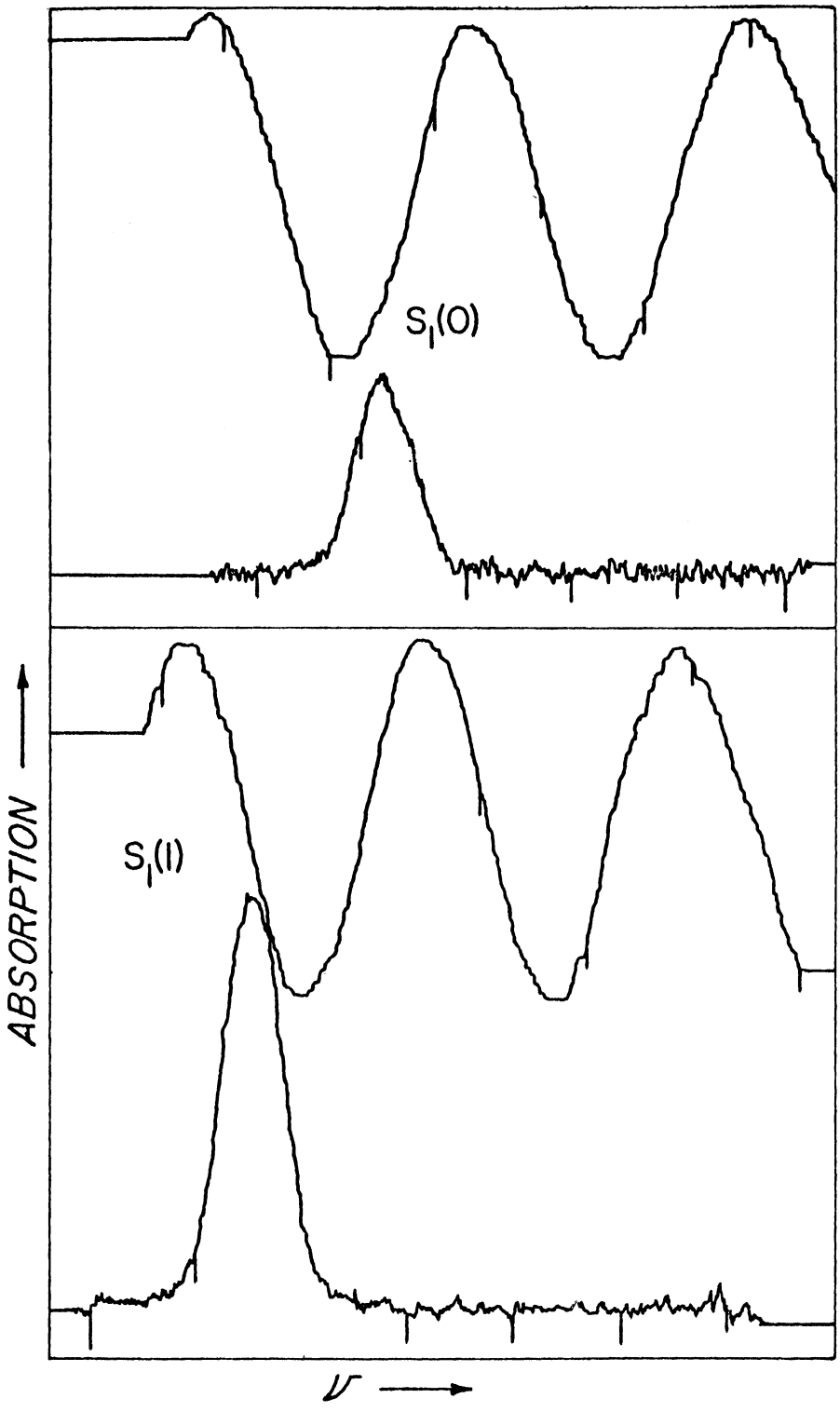

Fig. 10. $S_1(0)$ and $S_1(1)$ of ν_{0-1} of H_2. 86,000 volts/cm, 21 atm of H_2, 4-sec response, 0.2 cm^{-1} slits, fringe spacing 1.25 cm^{-1}.

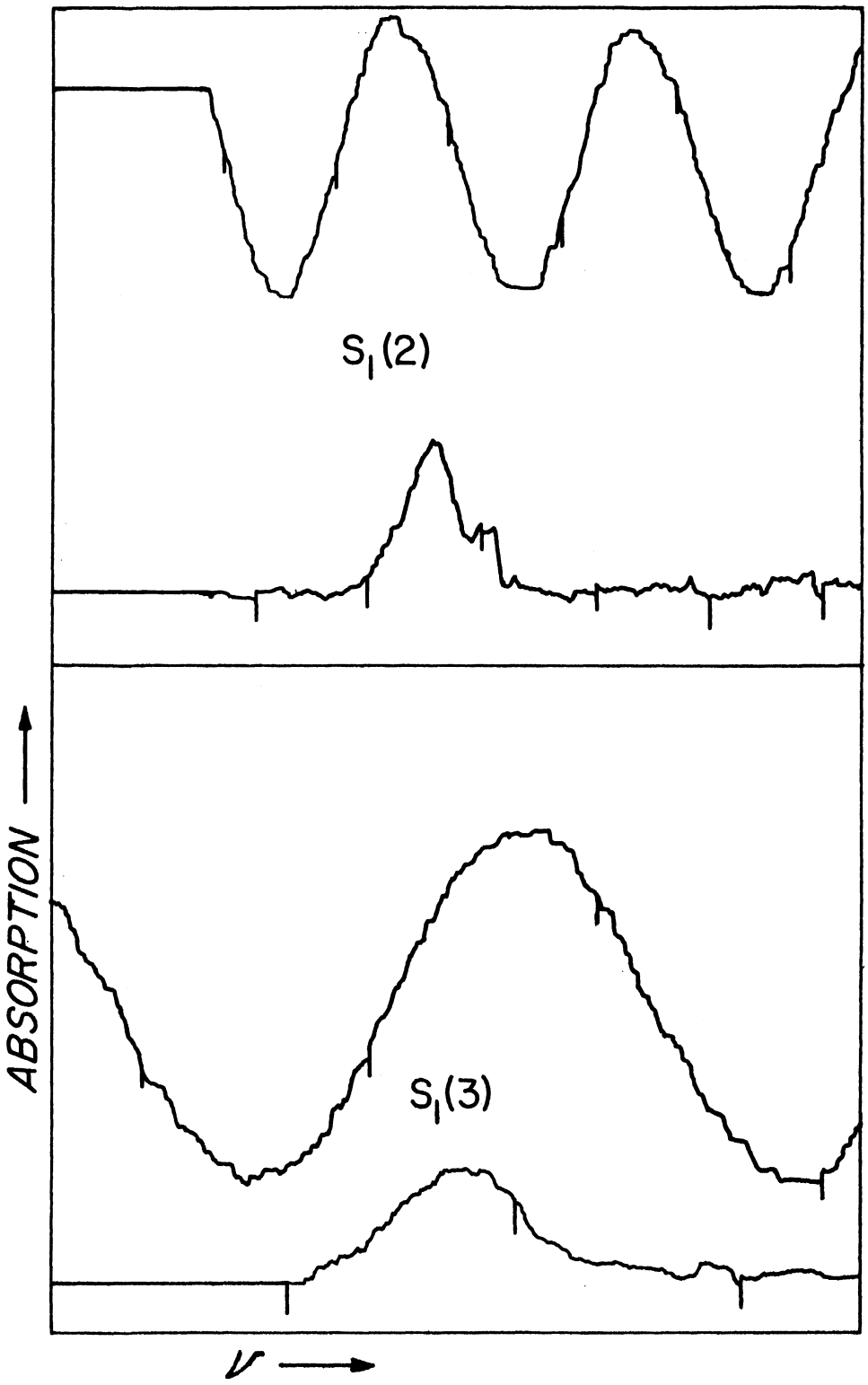

Fig. 11. $S_1(2)$ and $S_1(3)$ of ν_{0-1} of H_2. 86,000 volts/cm, 21 atm of H_2, 4-sec response for $S_1(2)$, 16-sec response for $S_1(3)$, slits 0.2 cm^{-1}, fringe spacing 1.25 cm^{-1}.

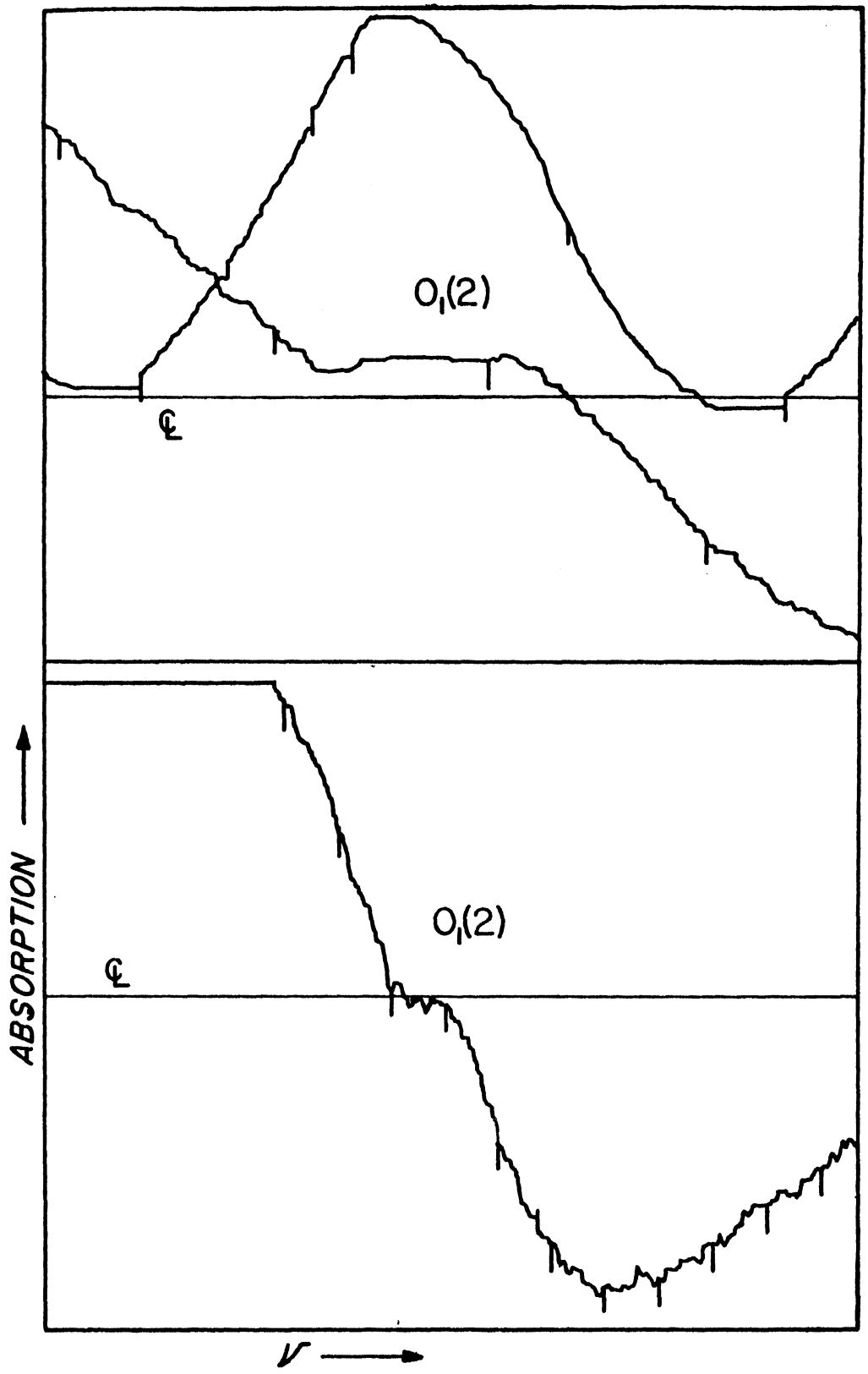

Fig. 12. $O_1(2)$ of ν_{0-1} of H_2. 92,000 volts/cm, 21 atm of H_2, 4-sec response on bottom, 16-sec response on top, slits 0.2 cm^{-1}, fringe spacing 1.0 cm^{-1}.

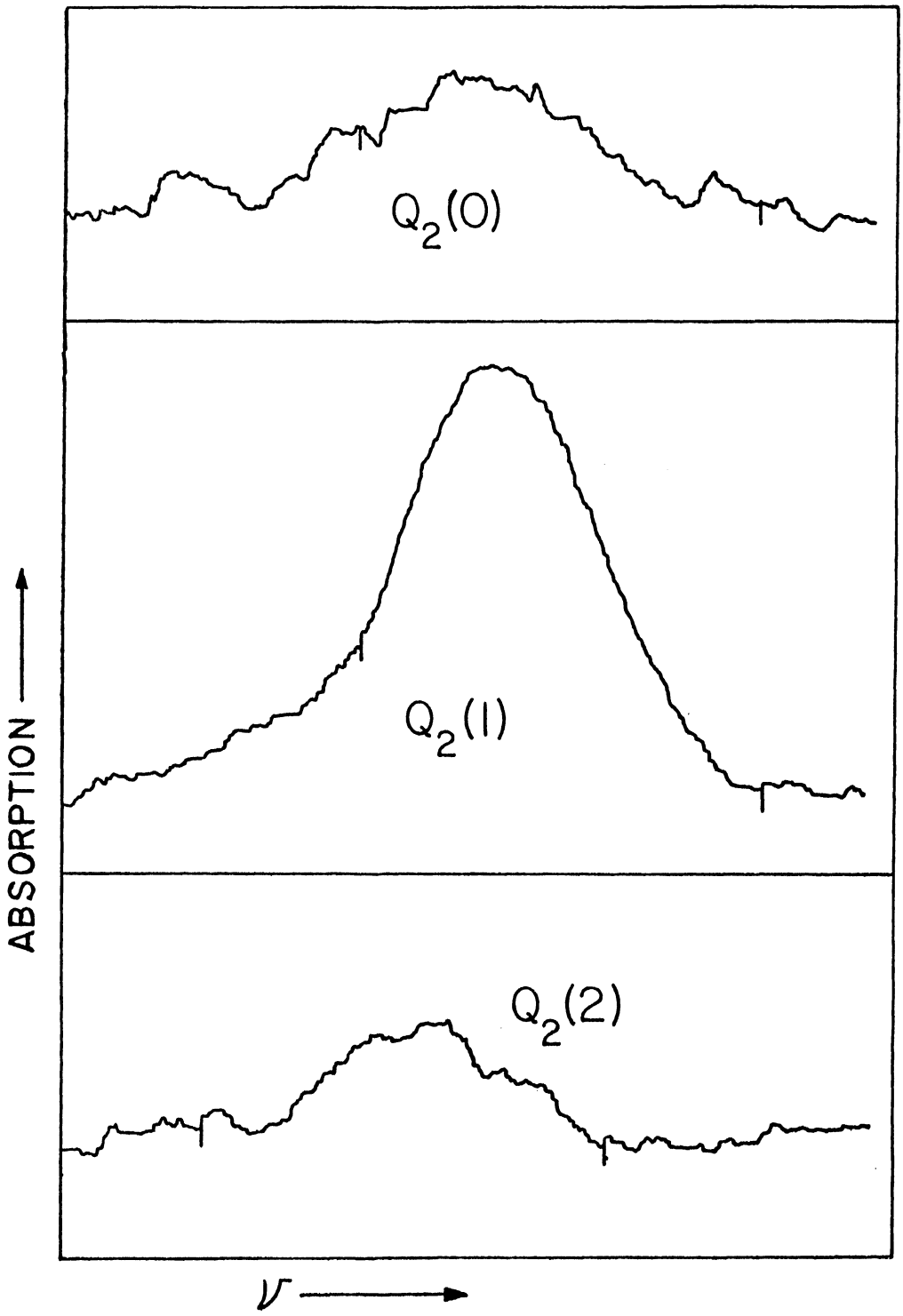

Fig. 13. $Q_2(0)$, $Q_2(1)$, and $Q_2(2)$ of ν_{0-2} of H_2. 91,000 volts/cm, 30 atm of H_2, 16-sec response, 0.4 cm^{-1} slits.

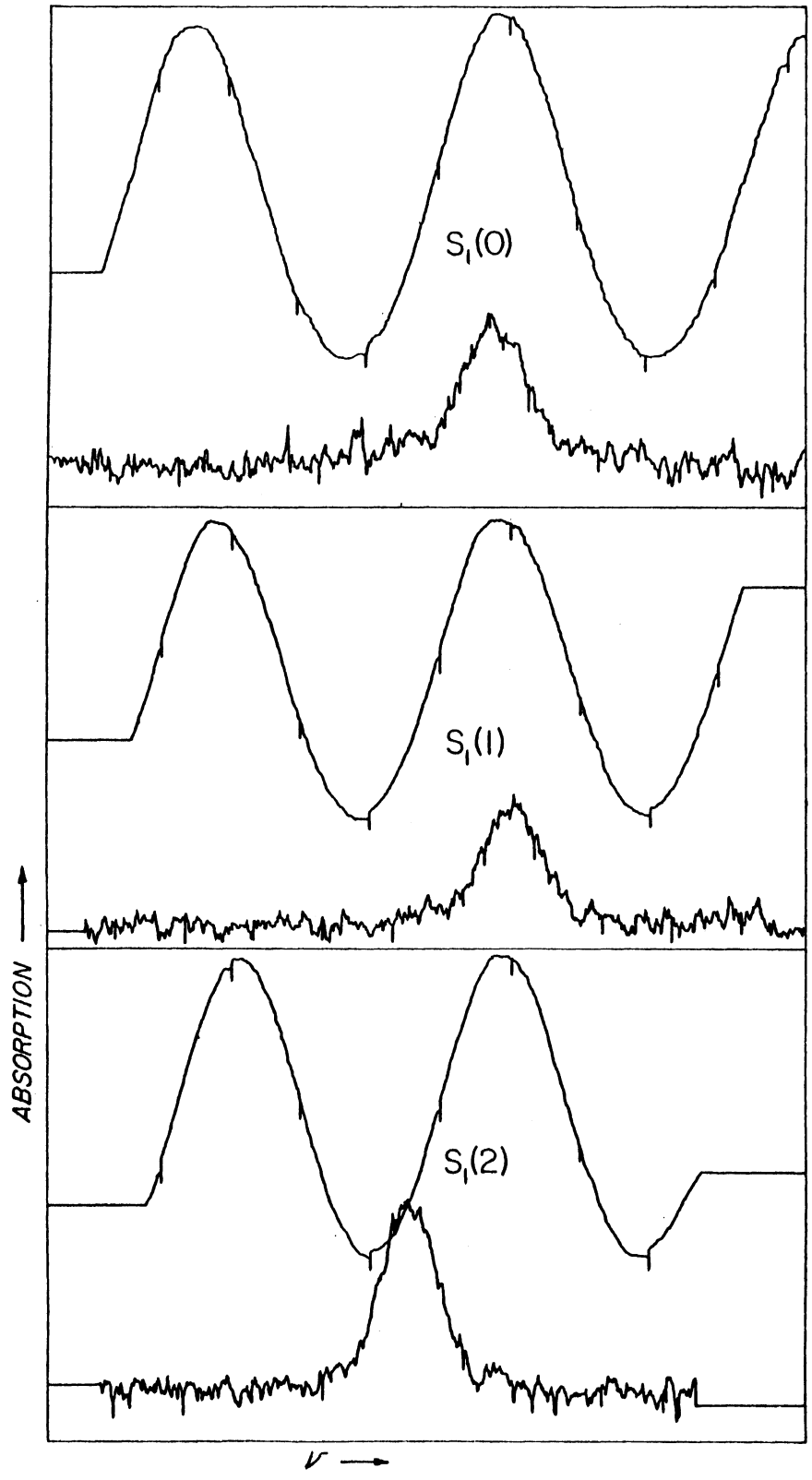

Fig. 14. $S_1(0)$, $S_1(1)$, and $S_1(2)$ of ν_{0-1} of D_2. 87,500 volts/cm, 21.5 atm of D_2, 4-sec response, 0.2 cm^{-1} slits, fringe spacing 1.0 cm^{-1}.

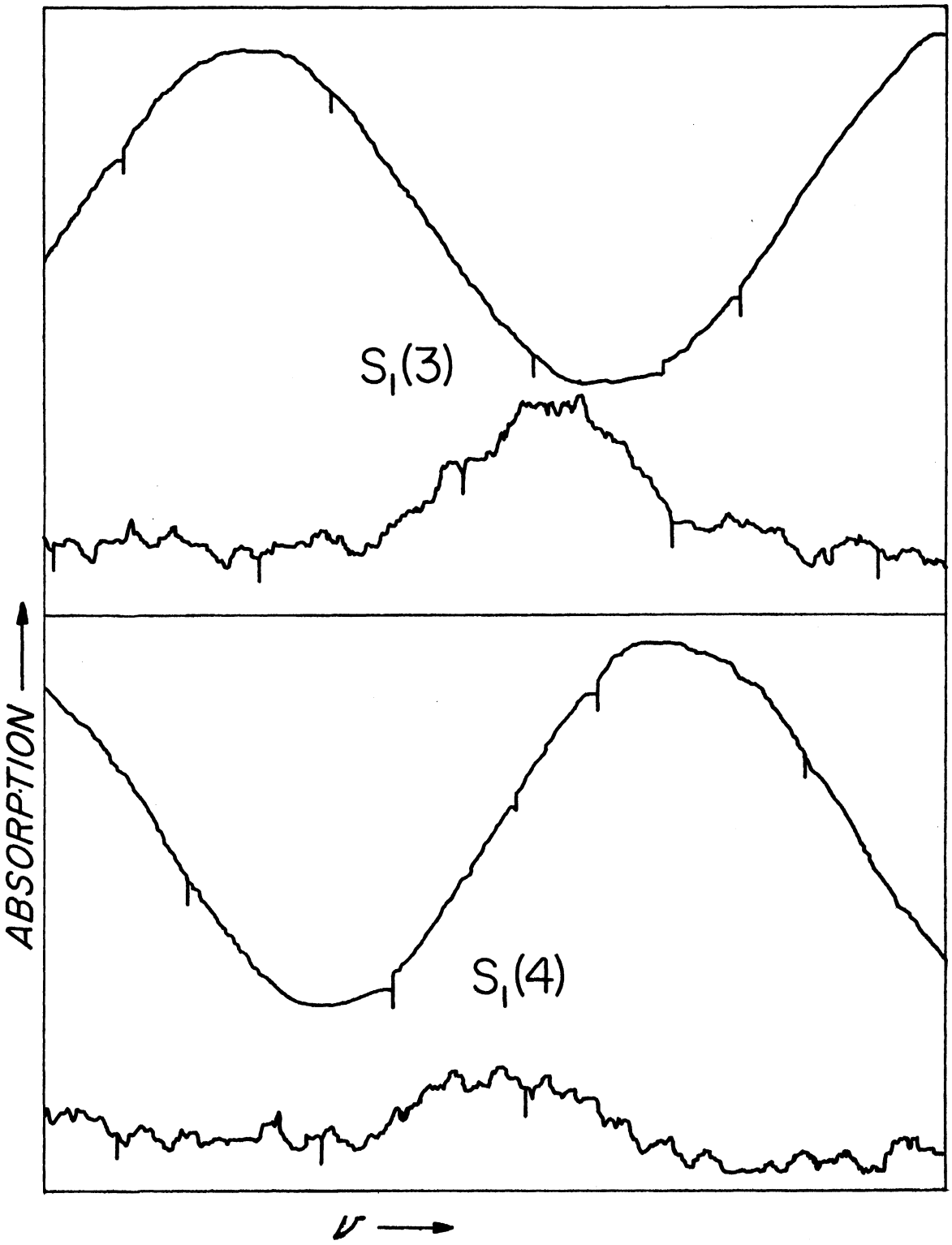

Fig. 15. $S_1(3)$ and $S_1(4)$ of ν_{0-1} of D_2. 87,500 volts/cm, 21.5 atm of D_2, 16-sec response, 0.22 cm^{-1} slits, fringe spacing 1.0 cm^{-1}.

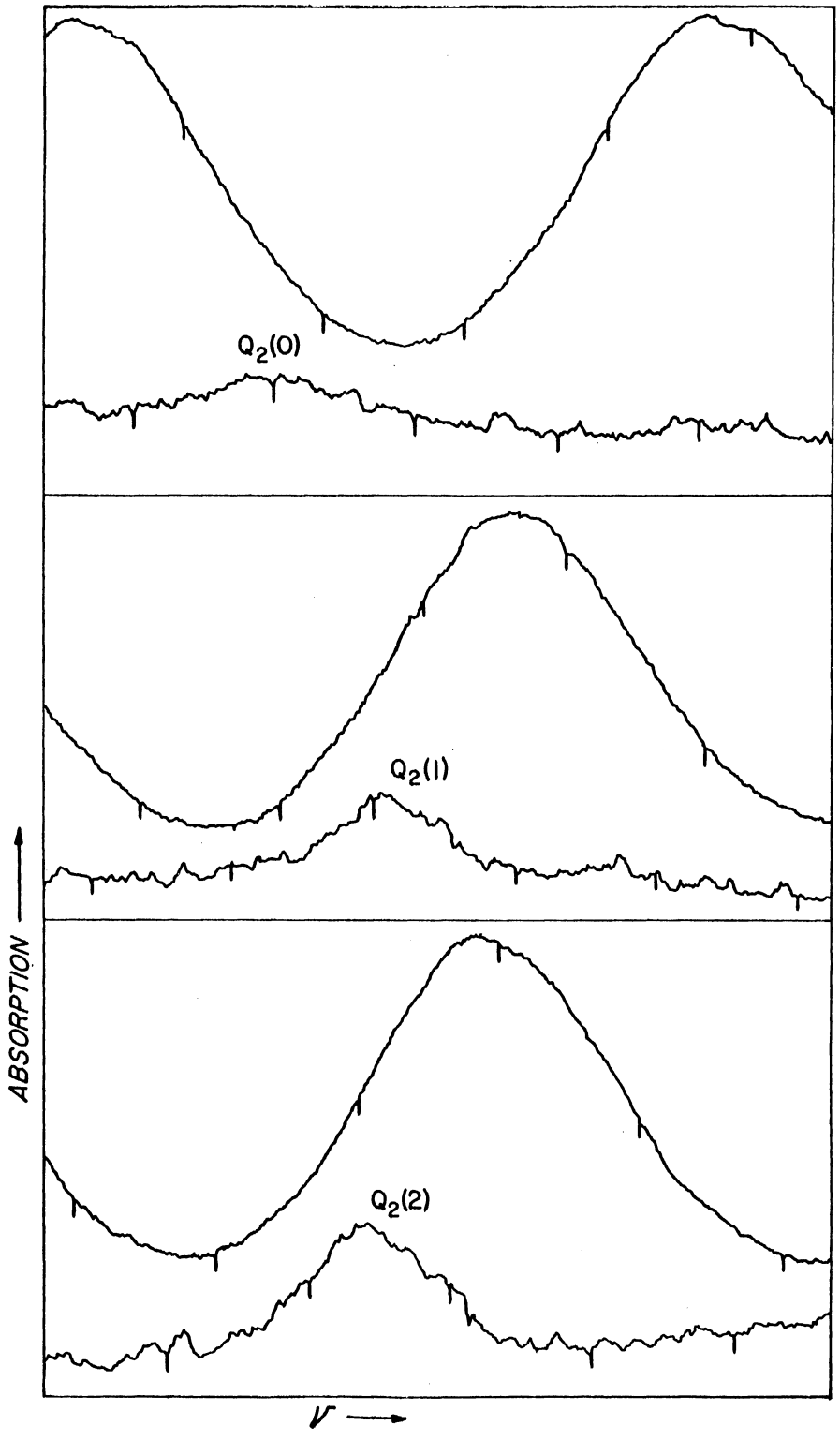

Fig. 16. $Q_2(0)$, $Q_2(1)$, and $Q_2(2)$ of ν_{0-2} of D_2. 97,000 volts/cm, 20.5 atm of D_2, 16-sec response, 0.3 cm^{-1} slits, fringe spacing 1.67 cm^{-1}.

spectrometer. These spectra are the actual recorder traces with the Fabry-Perot calibration fringes above. The fringe spacing was determined by the wave length of the light producing the fringes and by the spacing of the interferometer plates as discussed in Sec. 3.6. Figure 12 shows the only O branch line "observed." It is barely discernible as the flat break in the much larger intensity variation due to Stark modulation of a water vapor absorption line in the same region. The water vapor was present as an impurity in the H_2 in the cell since its absorption was modulated in the fashion noted by Terhune (3). It appeared as a first derivation of a normal line, with positive and negative excursions from zero as would be expected for a normal absorption line of a polar molecule broadened by the Stark effect. Unfortunately, a tank of extra dry H_2 was delivered empty due to a leaky valve, so that no further attempts were made to obtain better data on $O_1(2)$ or any other O_1 lines, all of which lie in range of strong H_2O absorption.

4.2 Line positions

The frequencies of all vibration-rotation transitions observed in this work are given for H_2 in Table V and for D_2 in Table VI. The probable error for most of the frequencies is $\pm$ 0.02 cm^{-1}, being somewhat larger (0.03 cm^{-1}) for weaker lines such as $Q_1(4)$

TABLE V

LINE POSITIONS OF H_2

Transition	Observed Value (cm^{-1})	Deviation of Calculated Frequency	
		Stoicheff (9)	Present
$Q_1(0)$[a]	4161.14	-0.01	0.000
$Q_1(1)$[a]	4155.21	-0.01	+0.001
$Q_1(2)$[a]	4143.43	-0.04	-0.002
$Q_1(3)$[a]	4125.85	-0.02	+0.002
$Q_1(4)$	4102.59	+0.15	+0.002
$Q_1(5)$	4073.73	+0.64	-0.007
$S_1(0)$	4497.81	-0.03	+0.003
$S_1(1)$	4712.81	+0.07	-0.008
$S_1(2)$	4916.82	-0.08	-0.015
$S_1(3)$	5108.26	-0.24	+0.010
$O_1(2)$	3807.3[b]	-0.55	-0.55
$Q_2(0)$	8086.88	+0.24	0.000
$Q_2(1)$[c]	8075.19	+0.20	+0.004
$Q_2(2)$	8051.86	+0.25	+0.007

[a]Observed by Stoicheff in Raman effect.

[b]Inaccurate due to interference by water vapor in cell.

[c]Observed by Herzberg by quadrupole absorption.

TABLE VI

LINE POSITIONS OF D_2

Transition	Observed Value (cm^{-1})	Deviation of Calculated Frequency	
		Stoicheff (9)	Present
$Q_1(0)^a$	2993.49	+0.06	0.000
$Q_1(1)^a$	2991.39	+0.06	-0.004
$Q_1(2)^a$	2987.18	+0.05	-0.002
$Q_1(3)^a$	2980.86	+0.02	+0.006
$Q_1(4)^a$	2972.46	+0.08	-0.010
$S_1(0)$	3166.22	+0.04	+0.005
$S_1(1)$	3278.43	-0.01	-0.019
$S_1(2)$	3387.20	0.00	-0.005
$S_1(3)$	3492.04	+0.09	+0.022
$S_1(4)$	3592.52	+0.25	+0.011
$Q_2(0)$	5867.66		0.00
$Q_2(1)$	5863.46		+0.02
$Q_2(2)$	5855.12		0.00

[a]Observed by Stoicheff in Raman effect.

and $Q_1(5)$ of H_2, and $S_1(3)$ and all Q_2 lines of both H_2 and D_2. The difference between the frequencies calculated from Stoicheff's constants and the observed frequencies is given, and shows sizable deviations (of 0.5 cm^{-1} or more) for the larger J values. A new set of molecular constants for H_2 and D_2 were calculated to best fit the present data, and the frequency differences between the calculated and observed frequencies are also included in Tables V and VI. For H_2, use was made of Herzberg's $Q_3(1)$ frequency to obtain $\omega_e y_e$. In D_2, this term was assumed zero for lack of reliable data.

In general, the observed frequencies differed from those calculated from Stoicheff's constants to an appreciable amount only for transitions involving the higher levels in both J and V. With respect to previously observed lines, only $Q_2(1)$ of the overtone band of H_2 showed a marked shift of 0.20 cm^{-1} from the quadrupole absorption spectra reported by Herzberg, well beyond the estimated error of 0.02 cm^{-1} in each measurement. (Actually, the ultraviolet electronic spectra yield values for all of these transitions, but, as mentioned earlier, the accuracy is at best one or more cm^{-1}.) It appeared conceivable, although improbable, that the electric field-induced transition could be shifted by a Stark effect. The magnitudes of the polarizability components indicated that such a shift would be of the order of 0.001 cm^{-1}. A sensitive experimental

check of a possible shift could be made by altering the square-wave modulation of the field from on-off to high-low. This could be done easily by inserting a capacitor in the ground wire to the spark gap so that the charge on the plates of the absorption cell was partially drained off to raise the inserted capacitor to an equal voltage. The phase-sensitive rectification rendered any absorption during the low-field half-cycle as a negative signal, and the difference between the positive and negative rectified signals was recorded. If there were a shift in line position with field strength, the positive and negative signals would be displaced and the recorder trace would be asymmetric. Observations of both the $Q_1(1)$ and $Q_2(1)$ lines showed no detectable asymmetry. This was tried with various values of the capacitors to obtain different field strengths ($2^{-1/2}$ E_{max} was considered optimum), and it was estimated from the intensities of the positive and negative signals that a shift of 0.01 cm would have been readily apparent. It would appear that Herzberg's measurement of the $Q_2(1)$ is in error, and this does not seem unreasonable in view of the weakness of the line image at the long wave length limit of the photographic plate.

The only previous information on the overtone of D_2 was from the electronic ultraviolet spectra reported by Jeppeson (7). Although

Jeppeson's values are considerably less accurate, the agreement is well within the experimental error tolerance.

4.3 Molecular constants

A new set of molecular constants describing the vibrational and rotational energies is given in Table VII for both H_2 and D_2, the terms being identified by equations 26 to 29 . Stoicheff's values of these constants are also given where available. One would think that a check on the accuracy of these constants would be furnished by the isotopic condition:

$$\frac{\mu_{D_2}}{\mu_{H_2}} = \frac{[B_e]_{H_2}}{[B_e]_{D_2}} = \frac{[\omega_e^2]_{H_2}}{[\omega_e^2]_{D_2}}$$

where μ is the reduced mass. However, in the case of hydrogen particularly, small corrections must be applied to B_e and ω_e to reach the "true" equilibrium state for which the ratios should hold exactly. A correction due to vibration-rotation interaction calculated by Dunham (43) increases both ω_e and B_e. Similarly, Van Vleck (44) calculated electronic interactions affecting the ground state of the hydrogen molecule and found that these also served to increase the value of ω_e and B_e. The "true" equilibrium constants obtained after these corrections are: for H_2, $\omega_e^* = 4405.40\ cm^{-1}$ and $B_e^* = 60.850\ cm^{-1}$; and for D_2, $\omega_e^* = 3114.15\ cm^{-1}$ and $B_e^* = 30.451\ cm^{-1}$.

TABLE VII

MOLECULAR CONSTANTS OF H_2 AND D_2

Item	H_2		D_2	
	Present	Stoicheff	Present	Stoicheff
ω_e	4401.60	4400.390	3112.81	
$\omega_e x_e$ . . .	121.66	120.8148	59.66	
$\omega_e y_e$ . . .	0.88	0.72419		
B_e	60.8496	60.8407	30.434	30.442[a]
α_e	3.0438	3.01774	1.061	1.0623
γ_e	0.0792	0.02855	0.009	
D_e	0.04955	0.046841	0.01085	0.01164[a]
β_e	-0.00395	-0.001706	0.0	0.00059[a]
δ	0.00087	0.0000308	0.0	
H_0	9.6×10^{-5}	5.2×10^{-5}	1×10^{-6}	
H_1	7.9×10^{-5}	5.2×10^{-5}	1×10^{-6}	
H_2	7.0×10^{-5}	5.2×10^{-5}	1×10^{-6}	
ν_{0-1}	4161.14	4161.137	2993.49	2993.561
ν_{0-2}	8086.88	8087.112	5867.66	
ν_{0-3}	11782.50[b]	11782.352		

[a] Estimated.

[b] Derived from Herzberg's value of $Q_3(1)$.

Using atomic masses from the American Institute of Physics Handbook of 1957, the values of the ratios are given in Table VIII. The ratio of the reduced masses of the molecules considering only the nuclei is also listed. At first glance, the uncorrected data appear to fit nicely, but an estimation of the probable errors shows that this is fortuitous. B_e of H_2 is thought accurate to 0.005 cm^{-1} (1 part in 10,000); B_e of D_2 to 0.01 cm^{-1} (1 part in 3,000), so that the error in their ratio is about ±0.001. The values of ω_e are more reliable, but ω_e is dependent upon changes in the vibrational frequencies, by the relation:

$$\Delta\omega_e = 5.9\,\Delta(\nu_{0-1}) - 3.87\,\Delta(\nu_{0-2}) + .96\,\Delta(\nu_{0-3})$$

For H_2 this leads to an estimated uncertainty of 5 parts in 100,000 for ω_e. For D_2, the absence of a reliable value of ν_{0-3} leads to a large uncertainty. In the calculations here $\omega_e y_e$ of D_2 was assumed to be negligible. However, Jeppeson's electronic spectra data showed that it is appreciable. This could lead to an error in ω_e of D_2 as large as 1 part in 1,000. When Jeppeson's value of ν_{0-3} is used with the present data to evaluate a modified ω_e' for D_2 (3115.83 cm^{-1}), the ratio of the square of the H_2 and D_2 frequencies is reduced quite a bit below the reduced mass ratio, and the interaction corrections then bring the ratio closer to the reduced

TABLE VIII

ISOTOPE EFFECT ON ω_e AND B_e OF H_2 AND D_2

Reduced Mass Ratio

Atomic masses: $\dfrac{\mu_{D_2}}{\mu_{H_2}} = 1.99846 \pm 0.00001$

Nuclear masses: $\dfrac{\mu_{d_2}}{\mu_{p_2}} = 1.99901 \pm 0.00001$

Ratio of Equilibrium Values from Present Data

$$\frac{[\omega_e^2]_{H_2}}{[\omega_e^2]_{D_2}} = 1.99948 \qquad \frac{[B_e]_{H_2}}{[B_e]_{D_2}} = 1.99940$$

Ratio of Corrected Equilibrium Values

$$\frac{[\omega_e^{*2}]_{H_2}}{[\omega_e^{*2}]_{D_2}} = 2.00121 \qquad \frac{[B_e^*]_{H_2}}{[B_e^*]_{D_2}} = 2.00055$$

Ratio with $[\omega_e]_{D_2}$ Modified by $\omega_e y_e$ Term from Jeppeson's Electronic Spectra Data

$$\frac{[\omega_e{}^2]_{H_2}}{[\omega_e'{}^2]_{D_2}} = 1.99560 \qquad \frac{[\omega_e{}^{*2}]_{H_2}}{[\omega_e'{}^{*2}]_{D_2}} = 1.99733$$

mass ratio. The situation is clearer for the H_2-HD isotopes, which were treated by Stoicheff, and for which reasonably accurate vibrational data are available through v = 3. The uncorrected ω_e ratio squared is 1.33258; corrected for interactions it is 1.33325. The reduced mass ratio for the bare nuclei is 1.33311, and for the atoms 1.33299. The estimated error in ω_e of either H_2 or HD is 5 parts in 100,000, and in the ratio ±0.0001. The interaction corrections are of the order of several cm^{-1} and presumed accurate to several percent, so that the ω_e^* ratio is also probably good to ±0.0001. The differences in this case appear to be significant. The uncorrected ratio is out of line, and the corrected ratio agrees with the reduced mass ratio of the bare nuclei as predicted by Van Vleck. (Stoicheff's conclusion that the data were of insufficient accuracy evidently was caused by the use of inaccurate values of the reduced masses.) These differences are quite a bit larger for the H_2-D_2 isotopes, and the present data coupled with a reliable value of v_{0-3} of D_2 should show it clearly. Measurement of this second overtone could probably be best accomplished by a quadrupole absorption spectrum. It is perhaps possible to observe it through electric field-induced absorption, but improbable that it could be found by Raman scattering.

Crawford and MacDonald have reported in their static electric field studies that $Q_1(0)$ and particularly $Q_1(1)$ differ by the order of 0.1 cm^{-1} from Stoicheff's values. The line position was also observed to be slightly dependent upon the pressure. The present measurements show no indication of such effects and it is suggested that they arise from variations in the pressure-induced absorption background. It is very unlikely, however, that the slope of the broad pressure-induced absorption could be sufficient to shift the apparent center of a line when observed as in the present case by modulation of the field with narrow slit widths.

4.4 Intensities and polarizabilities

The experimental intensities shown in Table IX and Table X are in terms of the absorption strength, A, given by equation 20; all observed intensities were reduced to unit electric field, unit pressure, and the same source intensity and detector sensitivity. The predicted intensities are those calculated for unit pressure and electric field from equation 20 using polarizabilities determined from this work and listed in Table XI, both for unpolarized light and for light as polarized in this equipment. A comparison of the two shows the detrimental effect of this grating on the Q branch lines of H_2. Since α_{01} was measured from $Q_1(0)$, γ_{01}, from $S_1(1)$ for H_2 and

TABLE IX

INTENSITIES OF H_2 TRANSITIONS

Transition	Observed $A \times 10^{16}$[a]	Predicted (light polarized as in this equipment) $A \times 10^{16}$	Calculated (unpolarized light) $A \times 10^{16}$
$Q_1(0)$	35	35	73
$Q_1(1)$	135	160	390
$Q_1(2)$	32	31	59
$Q_1(3)$	27	26	53
$Q_1(4)$	1.3	1.2	2.5
$Q_1(5)$	0.27	0.28	0.58
$S_1(0)$	7.8	7.3	8.0
$S_1(1)$	23	23	26
$S_1(2)$	4.5	3.7	4.1
$S_1(3)$	2.1	2.7	3.1
$O_1(2)$	?	1.2	1.2
$Q_2(0)$	0.2	0.24	0.53
$Q_2(1)$	1.3	1.3	2.8
$Q_2(2)$	0.2	0.21	0.42

[a] A is the absorption strength for unit pressure and unit electric field strength per cm path as in equation 20 .

TABLE X

INTENSITIES OF D_2 TRANSITIONS

Transition	Observed $A \times 10^{16}$[a]	Predicted (light polarized as in this equipment) $A \times 10^{16}$	Calculated (unpolarized light) $A \times 10^{16}$
$Q_1(0)$	63.5	63.5	51.6
$Q_1(1)$	79.3	75.5	60.6
$Q_1(2)$	146	140	113
$Q_1(3)$	51	41.4	33.5
$Q_1(4)$	28	34.4	27.7
$S_1(0)$	5.8	5.80	5.65
$S_1(1)$	4.3	4.05	3.99
$S_1(2)$	6.7	6.64	6.58
$S_1(3)$	1.0	1.87	1.86
$S_1(4)$	0.88	1.53	1.53
$Q_2(0)$	0.4	0.70	0.60
$Q_2(1)$	0.8	0.83	0.70
$Q_2(2)$	1.54	1.54	1.30

[a] A is the absorption strength for unit electric field strength per atmosphere pressure per cm of path as in equation 20 .

TABLE XI

POLARIZABILITIES OF H_2 AND D_2

Investigation	α_{01} $\times 10^{25}$ cm^3	γ_{01} $\times 10^{25}$ cm^3	α_{02} $\times 10^{25}$ cm^3	Method
		H_2		
Present work	0.97	0.78	0.06	AC electric field
Terhune	0.9	0.72		AC electric field
Crawford and MacDonald	0.97	0.72		DC electric field
Stansbury et al., and Cabannes and Rousset	1.05			Photographic Raman
Yoshino and Bernstein	0.985	0.75		Photoelectric Raman
Ishiguro et al.	1.39	0.90		Theoretical
		D_2		
Present work	0.81	0.66	0.06	AC electric field
Terhune	0.8	0.65		AC electric field
Stansbury et al. . . .	0.80	0.90		Photographic Raman
Yoshino and Bernstein	0.89[a]	0.68		Photoelectric Raman
Ishiguro et al.	1.13	0.71		Theoretical

[a]Uncertain in absolute units--measured relative to neopentane.

from $S_1(0)$ for D_2, and α_{02} from $Q_2(1)$ for H_2 and $Q_2(2)$ for D_2, these lines should agree exactly with the experimental values. The agreement for the other lines is good except for $Q_1(1)$ of H_2 and some of the very low-level lines. The former was absorbing so strongly under the conditions used that it was not in the linear range of the exponential law and it appeared weaker than it actually was.

The values of the polarizability components for H_2 and D_2 are recorded in Table XI. The value of α_{01} was determined from the absorption intensity of the $Q_1(0)$ line which has no dependence on γ_{01} (see equation [20] with the line strength $[S_0^0]_{11}^{01}$ from Table II). The γ_{01} was measured from the absorption intensity of the $S_1(1)$ line for H_2 and the $S_1(0)$ line for D_2 as the S branch lines depend only upon γ_{01} and not on α_{01} (see equation [20] with $[S_J^{+2}]_{11 \text{ or } \perp}^{01}$ from Table II). The ratio of α_{01} to γ_{01} was also measured by comparing the absorption strengths of $Q_1(0)$ and $S_1(J)$ for the same electric field and gas pressure. The absorption strength includes corrections for the polarization and dispersion of the grating, and for the relative signal-to-noise ratios due to changing source intensity and detector sensitivity. Both α_{01} and γ_{01} were accurate to about 3 percent; the major source of error was in reading the voltages on the oscilloscope trace. The measurement of α_{02} is accurate to

about 10 percent; it was complicated by a number of factors: (a) the overtone lines are weak; (b) the filters used to isolate the second order in which they were run were not wholly satisfactory; and (c) the lines measured (the strongest ones) depended upon both α_{02} and γ_{02}, the latter only to a small degree. The ratio of γ_{02}/α_{02} was taken to be about equal to γ_{01}/α_{01}; this assumption checked with the values in the paper of Ishiguro et al. (14).

Terhune's (3) values for α_{01} and γ_{01} are listed for comparison. The α_{01}'s for H_2 and D_2 obtained by Stansbury et al. (10) from the ratio of Rayleigh to Raman scattering when expressed as the matrix element (equation [13]) used here agree with these values. If the value for α_{00} of H_2 is taken to be 8.05×10^{-25} cm^3 as would be calculated from the dielectric constants of Maryott and Buckley (45) rather than the 8.4×10^{-25} cm^3 used by Stansbury et al., the agreement for H_2 would be even better. The γ_{01} calculated using equation (22) from the depolarization ratios of the Raman scattering are also given; the H_2 data are from Cabannes and Rousset (21) as corrected by Stansbury et al., who took D_2 to have the same depolarization ratio. The agreement with the photoelectric Raman values reported by Yoshino and Bernstein (11) is very close for both α_{01} and γ_{01} of H_2 and D_2. Likewise, the present result for α_{01} of H_2 is equal to that determined by a static electric field absorption

measurement by Crawford and MacDonald (13). The slight disparity between their value of γ_{01} and that reported here could be attributed to their difficulty in measuring the intensity of the very weak S line in the presence of background absorption. The theoretical values calculated by Ishiguro et al. (14) deviate considerably for α_{01} of both H_2 and D_2, and somewhat less for γ_{01}. They quote an accuracy of several percent for α_{00} and γ_{01}, and reasonably α_{01} and γ_{01} would be expected to have a much greater error.

4.5 Summary

A high-resolution study of the vibration-rotation transitions of a normally nonabsorbing molecule induced by a strong square-wave modulated electric field has been shown to yield more complete data of equal or better accuracy than available by other means both with respect to line frequencies and intensities. Several Q lines of the overtone were observed for H_2 and D_2, along with approximately five lines in the Q and S branches of the fundamental of each molecule. A new set of molecular constants was calculated to best fit the data, but the values for D_2 were notably inferior to those of H_2 for both the vibrational and the rotational constants. The polarizability components α_{01}, γ_{01}, and α_{02} were evaluated from the absolute absorption intensities of the lines, and they agreed within

experimental error (3 percent) with the recent photoelectric Raman determination.

One possible area in which these results might be applied concerns the existence of strong electric fields in the atmosphere--either of the earth or of the sun. If such were the case, for sufficiently low path lengths with a finite concentration of molecular hydrogen the absorption might be detected in the infrared solar spectrum. An examination of the solar spectrum atlas prepared by Mohler, Pierce, McMath, and Goldberg (46) shows no indication of the presence of any molecular hydrogen Q lines. It is thought, however, that the signal strength in the solar spectrum is large enough so that absorption considerably below the 1 percent value observable from the above atlas could be detected experimentally.

A number of changes could be made in the apparatus to improve the accuracy and detectability, factors that are relevant especially in the determination of the vibrational overtones. The measurement of line position is at present limited by temperature fluctuations that affect both the grating drive and the calibration of the Fabry-Perot etalon. In addition, there is an erratic linkage in the grating drive which is very bothersome irregularly. A higher signal-to-noise level could be almost certainly found by selecting the most sensitive PbS cell from an assortment. This is particularly

true for the region of the Q branch of the fundamental of D_2. A slower chopping frequency would probably also yield a gain in signal-to-noise for PbS cells cooled to liquid nitrogen temperature. Additional factors are available by using a longer slit length of the spectrometer, and by using a slower response time. A longer absorption cell would be indicated to improve the detectability of weak absorptions, although one must be careful here. Since most of the observations are of Q branch lines which absorb principally radiation with its electric vector parallel to the applied field, any polarizing effect in the system may be quite important. Unfortunately, because of Fresnel's reflection laws, the cell transmits $E_{\perp}$ more freely than $E_{\parallel}$, and a lengthened cell may actually decrease the sensitivity.

The polarization properties of the diffraction grating enter the problem in a similar way, and for optimum detection of Q lines the grating selected with the present apparatus should be used in the region of maximum efficiency for radiation polarized perpendicular to the grooves.

A more significant change could apparently be realized by the use of a cooled absorption cell. A higher density would be obtained for the same pressure, so that the absorption would be increased. Because of the higher density, the electric field strength

could be raised. The lines would be narrower, and by the Boltzman distribution the low J lines would be strengthened. In addition, for H_2 it would be possible to use enriched parahydrogen to increase the intensity of the Q(0) lines. Some slight gain would result from a corresponding reduction in the pressure-induced background. Finally, the substitution of a Fabry-Perot scanning interferometer as a spectrometer in place of the grating would yield a vastly higher level of radiation flux, so that still smaller changes in absorption could be detected with the proviso that the detector does not saturate.

Some of these changes require only minor alterations, others major revisions of the apparatus. It is felt that an order of magnitude increase in detectability can be realized relatively easily, and that a second order of magnitude increase is available with the expenditure of considerable effort.

Another area in which electric field-induced spectra may be of value concerns infrared inactive but Raman active transitions in liquids and solids. The Raman scattering intensity in dense phases is not proportional to the density but depends instead upon fluctuations in the density and is consequently weak. The induced absorption intensity, however, is directly proportional to the density for weak absorption. Furthermore, liquids and solids that are nonconducting possess a high dielectric strength so that considerably higher

electric fields may be applied without breakdown. These factors should combine to increase the detectability of induced absorption by several orders of magnitude over that of a gas, and should permit observation of such transitions even with thermal detectors.

BIBLIOGRAPHY

1. E. U. Condon, Phys. Rev. 41, 759 (1932).

2. M. F. Crawford and I. Dagg, Phys. Rev. 91, 1569 (1953).

3. R. W. Terhune, "Electric Field Induced Vibration-Rotation Spectra of H_2 and D_2," Thesis, Univ. of Mich. (1957).

4. L. A. Woodward, Nature 165, 198 (1950).

5. G. Placzek, Marx's Handbuch der Radiologie, 6th ed., part II, pp. 205-374, Akad. Verlags Gesellschaft MBH, Leipzig (1934).

6. C. R. Jeppeson, Phys. Rev. 44, 165 (1933).

7. C. R. Jeppeson, Phys. Rev. 49, 797 (1936).

8. G. Herzberg, Physics in Canada 13, 8 (1957).

9. B. P. Stoicheff, Can. J. of Phys. 35, 730 (1957).

10. E. J. Stansbury, M. F. Crawford, and H. L. Welsh, Can. J. of Phys. 31, 954 (1953).

11. T. Yoshino and H. J. Bernstein, J. of Mol. Spect. 2, 213 (1958).

12. G. Herzberg, Can. J. of Phys. 28, 144 (1950).

13. M. F. Crawford and R. E. MacDonald, Can. J. of Phys. 36, 1022 (1958).

14. E. Ishiguro, T. Arai, M. Mizushima, and M. Kotani, Proc. Phys. Soc. London A65, 178 (1952).

15. E. U. Condon and G. Shortley, Theory of Atomic Spectra, Cambridge Univ. Press, London (1935).

16. G. Herzberg, Spectra of Diatomic Molecules, 2d ed., Van Nostrand, New York (1950).

17. S. Bhagavantam, Scattering of Light and the Raman Effect, Andhra Univ., Waltair, India (1940).

18. G. Placzek and E. Teller, Zeits. f. Physik 81, 209 (1933).

19. S. Bhagavantam, Indian J. Phys. 7, 107, 549 (1932).

20. S. Bhagavantam, Proc. Indian Acad. Sc. 2, Sect. A, 303, 477 (1935).

21. J. Cabannes and A. Rousset, Comptes Rendus 206, 85 (1938).

22. R. P. Bell, Trans. Faraday Soc. 38, 422 (1942).

23. J. M. Meek and J. D. Craggs, Electrical Breakdown of Gases, Oxford Univ. Press, London (1953).

24. R. S. Mautner and O. H. Schade, RCA Review 8, 43 (1947).

25. "Reference Data for Radio Engineers," 4th ed., Int. Tel. and Telg. Corp., New York (1956).

26. H. W. Marshall, Jr., to be published.

27. D. E. Brown, "High Resolution Infrared Spectroscopy," Thesis, Univ. of Mich. (1957).

28. W. Fastie and W. Sinton, J. Opt. Soc. Am. 44, 103 (1954).

29. C. W. Peters and T. F. Zipf, to be published.

30. J. R. Platt, J. Opt. Soc. Am. 46, 609 (1956).

31. A. E. Douglas and D. Sharma, J. Chem. Phys. 21, 448 (1953).

32. E. K. Plyler, L. R. Blaine, and E. D. Tidwell, J. Res. Nat. Bur. Stds. 55, 279 (1955).

33. "Glass Color Filters," Corning Glass Works, Corning, New York (1948).

34. D. H. Rank and J. M. Bennett, J. Opt. Soc. Am. 45, 46 (1955).

35. W. F. Meggers and C. J. Humphreys, J. Res. Nat. Bur. Stds. 13, 293 (1934).

36. B. Edlen, J. Opt. Soc. Am. 43, 339 (1953).

37. D. H. Rank and J. N. Shearer, J. Opt. Soc. Am. 44, 375 (1954).

38. D. H. Rank, A. H. Guenther, G. D. Saksena, J. N. Shearer, and T. A. Wiggins, J. Opt. Soc. Am. 47, 686 (1957).

39. H. M. Crosswhite and G. H. Dieke, Am. Inst. Phys. Handbook, McGraw-Hill, New York (1957).

40. Private communication from J. Hickmott and R. Terhune.

41. R. J. Wylie, J. Sci. Inst. 31, 382 (1954).

42. H. L. Welsh, M. F. Crawford, and J. L. Locke, Phys. Rev. 76, 580 (1949).

43. J. L. Dunham, Phys. Rev. 41, 721 (1932).

44. J. H. Van Vleck, J. Chem. Phys. 4, 327 (1936).

45. A. A. Maryott and F. Buckley, Nat. Bur. Stds. Circular No. 537 (1953).

46. O. C. Mohler, A. K. Pierce, R. R. McMath, and L. Goldberg, Atlas of the Infrared Solar Spectrum, Univ. of Mich. Press, Ann Arbor (1950).